Achievable Angles Between Two Compressed Sparse Vectors Under Norm/Distance Constraints Imposed by the Restricted Isometry Property: A Plane Geometry Approach

Ling-Hua Chang and Jwo-Yuh Wu

***Abstract*—The angle between two compressed sparse vectors subject to the norm/distance constraints imposed by the restricted isometry property (RIP) of the sensing matrix plays a crucial role in the studies of many compressive sensing (CS) problems. Assuming that 1) u and v are two sparse vectors with $\measuredangle(\mathbf{u},\mathbf{v})=\theta$ and 2) the sensing matrix $\mathbf{\Phi}$ satisfies RIP, this paper is aimed at analytically characterizing the achievable angles between $\mathbf{\Phi u}$ and $\mathbf{\Phi v}$. Motivated by geometric interpretations of RIP and with the aid of the well-known law of cosines, we propose a plane-geometry-based formulation for the study of the considered problem. It is shown that all the RIP-induced norm/distance constraints on $\mathbf{\Phi u}$ and $\mathbf{\Phi v}$ can be jointly depicted via a simple geometric diagram in the 2-D plane. This allows for a joint analysis of all the considered algebraic constraints from a geometric perspective. By conducting plane geometry analyses based on the constructed diagram, closed-form formulas for the maximal and minimal achievable angles are derived. Computer simulations confirm that the proposed solution is tighter than an existing algebraic-based estimate derived using the polarization identity. The obtained results are used to derive a tighter restricted isometry constant of structured sensing matrices of a certain kind, to wit, those in the form of a product of an orthogonal projection matrix and a random sensing matrix. Follow-up applications in CS are also discussed.**

***Index Terms*—Compressive sensing (CS), plane geometry, restricted isometry constant (RIC), restricted isometry property (RIP).**

I. Introduction

A. Background and Motivation

COMPRESSIVE sensing (CS) is a new technique which exploits sparsity inherent in wide classes of real-world signals so as to facilitate efficient data acquisition, storage, and processing [1]–[3]. Applications of CS have been found in various areas, including analog-to-digital converters [4], magnetic resonance imaging [5], wireless communications [6]–[13], sensor networks [14], [15], and linear control [16]–[18], to name just a few. A CS system is typically described by an underdetermined linear equation set

$$\mathbf{y}=\mathbf{\Phi s} \tag{1.1}$$

where $\mathbf{s}\in\mathbb{R}^p$ is a K-sparse signal vector ($K\ll p$), $\mathbf{y}\in\mathbb{R}^m$ is the compressed measurement vector, and $\mathbf{\Phi}\in\mathbb{R}^{m\times p}$ is the sensing matrix with $m<p$. In the literature of CS, sufficient conditions for unique signal identification are commonly characterized in terms of the so-called restricted isometry property (RIP) of the sensing matrix [19], [20]. More precisely, the sensing matrix $\mathbf{\Phi}$ is said to satisfy the RIP of order K [19], [20] if there exists $0<\delta<1$ such that

$$(1-\delta)\left\|\mathbf{s}\right\|_2^2\le\left\|\mathbf{\Phi s}\right\|_2^2\le(1+\delta)\left\|\mathbf{s}\right\|_2^2 \tag{1.2}$$

holds for all K-sparse $\mathbf{s}$. In particular, for two sparse vectors $\mathbf{u}$ and $\mathbf{v}$ supported on T_u and T_v such that $|T_u\cup T_v|$, the cardinality of $T_u\cup T_v$, satisfies $|T_u\cup T_v|\le K$, it follows from (1.2) that

$$(1-\delta)\left\|\mathbf{u}-\mathbf{v}\right\|_2^2\le\left\|\mathbf{\Phi}(\mathbf{u}-\mathbf{v})\right\|_2^2\le(1+\delta)\left\|\mathbf{u}-\mathbf{v}\right\|_2^2. \tag{1.3}$$

Roughly speaking, if a sensing matrix $\mathbf{\Phi}$ satisfies RIP (1.2) with a small restricted isometry constant (RIC) δ, the information about x remains largely intact upon compression. In addition, (1.3) ensures that the Euclidean distance between two sparse vectors is approximately preserved in the compressed domain; this will guarantee robustness of signal recovery against noise perturbation. Both (1.2) and (1.3) characterize signal identifiability in terms of the norm, or Euclidean distance, of compressed sparse vectors. In the literature of CS, the angle $\measuredangle(\mathbf{\Phi u},\mathbf{\Phi v})$ between a compressed vector pair $\{\mathbf{\Phi u},\mathbf{\Phi v}\}$ plays an important role in many studies regarding stability analyses and performance evaluations. Specific examples include the following.

1) *Parameter Estimation with Compressed Measurements* [11]: In this problem, the angle $\measuredangle(\mathbf{\Phi u},\mathbf{\Phi v})$ is relevant to the assessment of the estimation errors. An upper bound on $|\measuredangle(\mathbf{\Phi u},\mathbf{\Phi v})-\measuredangle(\mathbf{u},\mathbf{v})|$ that is used for characterizing the estimation performance is given in [11, p. 454].
2) *Compressed Signal Detection* [12], [13]: In this problem, extreme values of $\measuredangle(\mathbf{\Phi u},\mathbf{\Phi v})$ is needed to characterize the

Manuscript received January 09, 2012; revised September 17, 2012; accepted December 03, 2012. Date of publication December 20, 2012; date of current version March 13, 2013. This work was supported in part by the National Science Council of Taiwan under Grants NSC 100-2221-E-009-104-MY3, NSC 100-2628-E-009-004, and NSC 101-2923-P-009-001-MY2, in part by the Ministry of Education of Taiwan under the MoE ATU Program, and in part by the Telecommunication Laboratories, Chunghwa Telecom Co., Ltd. under Grant TL-101-G106. This paper was presented in part at the 2012 IEEE Wireless Communications and Networking Conference 2012 and has been submitted to the 14th IEEE International Workshop on Signal Processing Advances in Wireless Communications.

The authors are with the Department of Electrical and Computer Engineering, National Chiao Tung University, Hsinchu 300, Taiwan, R.O.C. (e-mail: iamjaung@gmail.com; jywu@cc.nctu.edu.tw).

Communicated by M. Elad, Associate Editor for Signal Processing.

Color versions of one or more of the figures in this paper are available online at http://ieeexplore.ieee.org.

Digital Object Identifier 10.1109/TIT.2012.2234825

worst-case detection/missing probability [12]. Under the assumption that the sensing matrix satisfies the RIP and the value of RIC falls within a certain range, estimates of the achievable $\measuredangle(\mathbf{\Phi u}, \mathbf{\Phi v})$ have been provided in [13].

3) *Compressed-Domain Interference Cancellation* [9]–[11]: Under the assumption that the support of interference is known, the effective sensing matrix upon interference cancellation admits the form $\mathbf{P\Phi}$, where $\mathbf{P}$ is a certain orthogonal projection matrix and $\mathbf{\Phi}$ is a random sensing matrix. Assume that the commonly used l_1-minimization algorithm [19], [20] is adopted for signal recovery, and let $\hat{\mathbf{x}}$ be the reconstruction of the desired sparse signal vector $\mathbf{x}$. Based on [26, eqs. (5) and (6)], the upper bound of the reconstruction error is known to be

$$\|\hat{\mathbf{x}} - \mathbf{x}\|_2 \leq \frac{4(1+\bar{\delta})\varepsilon}{1-(\sqrt{2}-1)\bar{\delta}}$$

where $\bar{\delta}$ is the RIC of $\mathbf{P\Phi}$ and ε is the level of the data mismatch (measured in l_2-norm). To determine $\bar{\delta}$ so as to explicitly evaluate the reconstruction performance, a key step is to estimate the achievable angles between two orthogonal sparse vectors in the compressed domain; see Lemma 1 and Theorem 2 in [9].

4) *RIP-based Analyses of the Orthogonal Matching Pursuit (OMP) Algorithm* [21]–[24]: Structured sensing matrices of the form $\mathbf{P\Phi}$, the product of an orthogonal projection matrix $\mathbf{P}$ and a random sensing matrix $\mathbf{\Phi}$, also arise in modeling the residual vector of the OMP algorithm so as to facilitate RIP-based stability analysis [21], [22]. In particular, the RIC of $\mathbf{P\Phi}$ is needed to establish certain sufficient conditions for signal recovery. Hence, as mentioned previously, knowledge of the achievable angles between a pair of orthogonal sparse vectors upon compression is required; see also [21, Lemmas 3.2 and 3.3, p. 4398].

5) *Characterization of the Democratic Nature of Random Sensing Matrices* [25], [26]: The RIC of the structured sensing matrix $\mathbf{P\Phi}$ is also crucial for characterizing the robustness of random sensing/projection against measurement loss, a property termed as the "democratic nature" of random sensing matrices. To establish the main results therein, bounds of the achievable angles between two compressed sparse vectors with nonoverlapping supports are required; see the analyses in [25, Ths. 1 and 3].

In most of the aforementioned works, the analysis resorted to certain upper bounds of $|\cos(\measuredangle(\mathbf{\Phi u}, \mathbf{\Phi v}))|$ that are derived by using inequalities such as (1.2) and (1.3) in conjunction with the polarization identity.[1] The bounds obtained via such an algebraic-based RIP analysis, however, are the worst-case estimates [28] and will lead to a pessimistic judgment about the true system performance. Toward more accurate performance evaluations, a fundamental approach is to explicitly specifying the achievable $\measuredangle(\mathbf{\Phi u}, \mathbf{\Phi v})$ subject to the norm/distance constraints induced by RIP. In-depth studies of such problems, however, have not been seen in the literature yet.

[1]For $\mathbf{u}, \mathbf{v} \in \mathbb{R}^p$, the inner product between $\mathbf{u}$ and $\mathbf{v}$ can be expressed as $\langle \mathbf{u}, \mathbf{v} \rangle = \{\|\mathbf{u}+\mathbf{v}\|_2^2 - \|\mathbf{u}-\mathbf{v}\|_2^2\}/4$ [27].

B. Paper Contribution

This paper investigates the maximal and minimal achievable angles between two compressed sparse vectors under norm/distance constraints imposed by RIP. To be more precise, we consider two sparse vectors $\mathbf{u} \in \mathbb{R}^p$ and $\mathbf{v} \in \mathbb{R}^p$ whose supports T_u and T_v satisfy $|T_u \cup T_v| \leq K$. Suppose that the angle between $\mathbf{u}$ and $\mathbf{v}$ is $\measuredangle(\mathbf{u}, \mathbf{v}) = \theta$, that is,

$$\frac{\langle \mathbf{u}, \mathbf{v} \rangle}{\|\mathbf{u}\|_2 \|\mathbf{v}\|_2} = \cos\theta \tag{1.4}$$

where $0 < \theta \leq \pi/2$ is assumed without loss of generality.[2] In the compressed domain, the angle between $\mathbf{\Phi u}$ and $\mathbf{\Phi v}$ is $\measuredangle(\mathbf{\Phi u}\mathbf{\Phi v}) = \alpha$, i.e.,

$$\frac{\langle \mathbf{\Phi u}, \mathbf{\Phi v} \rangle}{\|\mathbf{\Phi u}\|_2 \|\mathbf{\Phi v}\|_2} = \cos\alpha. \tag{1.5}$$

Under RIP (1.2) and (1.3), all we know about $\mathbf{\Phi u}$ and $\mathbf{\Phi v}$ are the plausible values of the respective norms and distance. This implies that the measure of α (or the value of $\cos\alpha$) will lie within a certain range. Given a fixed $\measuredangle(\mathbf{u}, \mathbf{v}) = \theta$, we propose a method for identifying the maximal and the minimal achievable α, hereafter denoted respectively by[3] $\alpha_{\max}$ and $\alpha_{\min}$, subject to the RIP-induced norm/distance constraints. Specific technical contributions of this paper can be summarized as follows.

1) By exploiting geometric interpretations of RIP and the well-known law of cosines [29], [30], it is shown that the angle between a feasible pair $\{\mathbf{\Phi u}, \mathbf{\Phi v}\}$ has the same measure as the angle determined by one vertex of an auxiliary triangle in the two-dimensional *2-D plane*. This leads to a natural problem formulation on the basis of the plane geometry framework for the study of the achievable α. With the aid of the proposed formulation, we then leverage the technique of *similarity*[4] in plane geometry [29], [30] to construct a geometric diagram depicting all the auxiliary triangles associated with all feasible $\{\mathbf{\Phi u}, \mathbf{\Phi v}\}$. The problem then boils down to searching into the diagram for the two triangles whose corresponding vertices yield, respectively, the largest and smallest angles.

2) The distinctive features of the proposed *plane-geometry*-based formulation are twofold. First, all the RIP-induced algebraic norm/distance constraints that are relevant to the characterization of the angle $\measuredangle(\mathbf{\Phi u}, \mathbf{\Phi v})$ can be jointly elucidated in a visualizable manner from a plane geometry perspective. This facilitates a *joint* analysis of all the considered algebraic constraints in the plane geometry setting for the identification of $\alpha_{\max}$ and $\alpha_{\min}$. Such an approach is in marked contrast with the existing algebraic-based method [9], [21], [25], wherein the extreme values of the norm/distance specified by the inequalities (1.2) and (1.3) are employed to obtain mere the worst-case

[2]If the angle $\measuredangle(\mathbf{u}, \mathbf{v}) = \theta > \pi/2$, then consider instead, say, $\mathbf{u}$ and $-\mathbf{v}$ with $\measuredangle(\mathbf{u}, -\mathbf{v}) = \pi - \theta < \pi/2$. Since $\measuredangle(\mathbf{\Phi u}, \mathbf{\Phi v})$ and $\measuredangle(\mathbf{\Phi u}, -\mathbf{\Phi v})$ are supplementary, i.e., $\measuredangle(\mathbf{\Phi u}, \mathbf{\Phi v}) + \measuredangle(\mathbf{\Phi u}, -\mathbf{\Phi v}) = \pi$, the largest and smallest $\measuredangle(\mathbf{\Phi u}, \mathbf{\Phi v})$ can be directly obtained as the supplements of, respectively, the smallest and largest achievable $\measuredangle(\mathbf{\Phi u}, -\mathbf{\Phi v})$.

[3]The dependence of $\alpha_{\max}$ and $\alpha_{\min}$ on θ is omitted in the sequel to conserve notation.

[4]The technique of similarity has also been adopted in, e.g., algorithm development in the context of pattern recognition [31], [32].

estimate of α (or $\cos\alpha$). Second, by conducting plane geometry analyses based on the constructed geometric diagram, *closed-form* formulas of $\alpha_{\max}$ and $\alpha_{\min}$ can be derived and are then validated through computer simulations.

3) Applications of the obtained analytic results to CS are investigated. First of all, the achievable RIC of a structured sensing matrix of the form $\mathbf{P\Phi}$, where $\mathbf{P}$ is a certain orthogonal projection matrix and $\mathbf{\Phi}$ is a random sensing matrix, is investigated. Matrices of this kind were found in, e.g., compressed-domain interference cancellation [9]–[11], RIP-based analyses of the OMP algorithm [21], and characterization of the democratic nature of random sensing matrices [25], [26]. Based on the knowledge of $\alpha_{\max}$ and $\alpha_{\min}$, we derive a closed-form formula for the RIC of $\mathbf{P\Phi}$. The proposed solution is shown to be tighter than an existing estimate given in [9], [21], and [25]. The impact of our study on the interference cancellation problem has been reported in [33] and, thus, is omitted here to conserve space. Applications of this result to the last problem mentioned above are also discussed.

C. Connection to Previous Works

It is noted that, based on the plane geometry approach introduced in [34] and [35], bounds of the achievable angles between two compressed sparse vectors have also been derived in [12] and [13]. The main idea behind the method in [34] and [35] lies in the construction of auxiliary right and isosceles triangle in the ambient signal domain, followed by geometric characterizations of the transformed triangle upon the dimensionality-reduction mapping. Even though both our result and [12], [13] are developed under the plane geometry setting, the bounds given in [12] and [13] are valid only when the value of the RIC of the sensing matrix satisfies certain conditions. On the contrary, the solutions in our paper hold true without any requirements on the RIC. Numerical results also evidence that the proposed solutions in our paper can provide tighter estimates of the achievable angles; this will be seen in Section V.

The rest of this paper is organized as follows. Section II presents the proposed plane geometry based formulation. The maximal and minimal achievable angles are derived, respectively, in Sections III and IV. Section V discusses the connection between the presented analytic study with previous works; simulation results are also given to evidence the proposed analytic solutions. Section VI investigates the applications of the obtained results to CS. Section VII presents the conclusion. To ease reading, all supporting technical proofs of the established mathematical lemmas and theorems are relegated to the Appendix.

II. Proposed Plane-Geometry-Based Formulation

This section introduces the proposed plane-geometry-based analysis framework for identifying $\alpha_{\max}$ and $\alpha_{\min}$. After highlighting some intuitive motivations, Section II-A presents the proposed problem formulation. Section II-B constructs a geometric diagram in the 2-D plane that shows concrete geometric depictions of all the feasible $\measuredangle(\mathbf{\Phi u}, \mathbf{\Phi v})$ under RIP. Section II-C provides more explicit characterizations about $\alpha_{\max}$ and $\alpha_{\min}$ within the proposed plane geometry framework. The derivations of $\alpha_{\max}$ and $\alpha_{\min}$ will be given in Sections III and IV.

Recall that, under RIP (1.2) and (1.3), all we know about $\mathbf{\Phi u}$ and $\mathbf{\Phi v}$ is the maximal, and minimal, achievable norms and distance. To identify $\alpha_{\max}$ and $\alpha_{\min}$, the first step is to find a mathematical relation which can delineate the connection between the norm/distance information about the pair $\{\mathbf{\Phi u}, \mathbf{\Phi v}\}$ and the resultant angle $\measuredangle(\mathbf{\Phi u}, \mathbf{\Phi v}) = \alpha$. Hopefully, such a formula can moreover provide distinctive insights to facilitate an analytic study of the considered problem from a geometric perspective. The ideas above can be realized by the well-known law of cosines, which states that the angle $\measuredangle(\mathbf{\Phi u}, \mathbf{\Phi v}) = \alpha$ can be determined by $\|\mathbf{\Phi u}\|_2$, $\|\mathbf{\Phi v}\|_2$, and $\|\mathbf{\Phi}(\mathbf{u}-\mathbf{v})\|_2$ as

$$\cos\alpha = \frac{\|\mathbf{\Phi u}\|_2^2 + \|\mathbf{\Phi v}\|_2^2 - \|\mathbf{\Phi}(\mathbf{u}-\mathbf{v})\|_2^2}{2\,\|\mathbf{\Phi u}\|_2\,\|\mathbf{\Phi v}\|_2}. \tag{2.1}$$

Hence, at least conceptually, by taking account of all the available knowledge about $\|\mathbf{\Phi u}\|_2$, $\|\mathbf{\Phi v}\|_2$, and $\|\mathbf{\Phi}(\mathbf{u}-\mathbf{v})\|_2$ under RIP, it is possible to characterize the achievable α and, in particular, to identify $\alpha_{\max}$ and $\alpha_{\min}$. The unique advantage of (2.1) is its underlying geometric interpretation: we can think of $\|\mathbf{\Phi u}\|_2$, $\|\mathbf{\Phi v}\|_2$, and $\|\mathbf{\Phi}(\mathbf{u}-\mathbf{v})\|_2$ as the three sides of a triangle in $\mathbb{R}^m$, and $\measuredangle(\mathbf{\Phi u}, \mathbf{\Phi v})$ then has the same measure as the angle defined by a certain vertex of this triangle. As will be shown later, such a simple and concrete geometric view of $\measuredangle(\mathbf{\Phi u}, \mathbf{\Phi v})$ will allow for a natural problem formation within the plane geometry framework. We shall note that the angle between two vectors is invariant to scaling of the respective norms, that is, if $\mathbf{u}$ and $\mathbf{v}$ are such that $\measuredangle(\mathbf{u}, \mathbf{v}) = \theta$ and $\measuredangle(\mathbf{\Phi u}, \mathbf{\Phi v}) = \alpha$, then it follows $\measuredangle(c_1\mathbf{u}, c_2\mathbf{v}) = \theta$ and $\measuredangle(c_1\mathbf{\Phi u}, c_2\mathbf{\Phi v}) = \alpha$ regardless of any positive scalars c_1 and c_2 [see (1.4) and (1.5)]. Hence, we assume in the sequel that $\|\mathbf{u}\|_2 = \|\mathbf{v}\|_2 = 1$.

Before introducing the proposed formulation, let us first specify the relevant norm/distance information about $\mathbf{\Phi u}$ and $\mathbf{\Phi v}$ that is revealed by RIP. The plausible values of $\|\mathbf{\Phi u}\|_2^2$ and $\|\mathbf{\Phi v}\|_2^2$ under RIP (1.2) are

$$1-\delta \le \|\mathbf{\Phi u}\|_2^2 \le 1+\delta \text{ and } 1-\delta \le \|\mathbf{\Phi v}\|_2^2 \le 1+\delta. \tag{2.2}$$

Also, the achievable distance between $\mathbf{\Phi u}$ and $\mathbf{\Phi v}$ can be directly obtained from (1.3) and the law of cosines as

$$d_{\min}^2 \le \|\mathbf{\Phi}(\mathbf{u}-\mathbf{v})\|_2^2 \le d_{\max}^2 \tag{2.3}$$

in which

$$\begin{aligned} d_{\max}^2 &\triangleq (1+\delta)\,\|\mathbf{u}-\mathbf{v}\|_2^2 \\ &= (1+\delta)\cdot\left\{\|\mathbf{u}\|_2^2 + \|\mathbf{v}\|_2^2 - 2\,\|\mathbf{u}\|_2\,\|\mathbf{v}\|_2\cos\theta\right\} \\ &= 2(1+\delta)(1-\cos\theta) \end{aligned} \tag{2.4}$$

and

$$\begin{aligned} d_{\min}^2 &\triangleq (1-\delta)\,\|\mathbf{u}-\mathbf{v}\|_2^2 \\ &= (1-\delta)\cdot\left\{\|\mathbf{u}\|_2^2 + \|\mathbf{v}\|_2^2 - 2\,\|\mathbf{u}\|_2\,\|\mathbf{v}\|_2\cos\theta\right\} \\ &= 2(1-\delta)(1-\cos\theta). \end{aligned} \tag{2.5}$$

We note that the law of cosines (2.1) can also be expressed as

$$\begin{aligned}\cos\alpha &= -\cos(\pi-\alpha)\\ &= -\left(\frac{\|\mathbf{\Phi u}\|_2^2+\|\Phi\mathbf{v}\|_2^2-\|\Phi(\mathbf{u}+\mathbf{v})\|_2^2}{2\|\Phi\mathbf{u}\|_2\|\Phi\mathbf{v}\|_2}\right). \quad (2.6)\end{aligned}$$

Hence, in addition to $\|\mathbf{\Phi u}\|_2^2$, $\|\mathbf{\Phi v}\|_2^2$, and $\|\mathbf{\Phi}(\mathbf{u}-\mathbf{v})\|_2^2$, (2.6) implies that the knowledge of $\|\mathbf{\Phi}(\mathbf{u}+\mathbf{v})\|_2^2$ is also needed for characterizing $\cos\alpha$. As a result, the following constraint on $\|\mathbf{\Phi}(\mathbf{u}+\mathbf{v})\|_2^2$ imposed by RIP should also be taken into account:

$$\tilde{d}_{\min}^2 \le \|\mathbf{\Phi}(\mathbf{u}+\mathbf{v})\|_2^2 \le \tilde{d}_{\max}^2 \quad (2.7)$$

where

$$\begin{aligned}\tilde{d}_{\max}^2 &\triangleq (1+\delta)\|\mathbf{u}+\mathbf{v}\|_2^2\\ &= (1+\delta)\cdot\left\{\|\mathbf{u}\|_2^2+\|\mathbf{v}\|_2^2+2\|\mathbf{u}\|_2\|\mathbf{v}\|_2\cos\theta\right\},\\ &= 2(1+\delta)(1+\cos\theta) \quad (2.8)\end{aligned}$$

and

$$\begin{aligned}\tilde{d}_{\min}^2 &\triangleq (1-\delta)\|\mathbf{u}+\mathbf{v}\|_2^2\\ &= (1-\delta)\cdot\left\{\|\mathbf{u}\|_2^2+\|\mathbf{v}\|_2^2+2\|\mathbf{u}\|_2\|\mathbf{v}\|_2\cos\theta\right\}\\ &= 2(1-\delta)(1+\cos\theta). \quad (2.9)\end{aligned}$$

The conditions (2.2), (2.3), and (2.7) can be regarded as the full characterization of the norm/distance information about $\mathbf{\Phi u}$ and $\mathbf{\Phi v}$ under RIP. Our task is to find $\alpha_{\max}$ and $\alpha_{\min}$ based solely on (2.2), (2.3), and (2.7). The following notation will be used throughout the rest of this paper.

- $\overline{PQ}$: the line segment between the two points P and Q in the 2-D plane.
- $|\overline{PQ}|$: length of the line segment $\overline{PQ}$.
- ΔABC: the triangle with three vertexes denoted by A, B, and C.
- $\measuredangle ABC$: the angle with $\overline{BA}$ and $\overline{BC}$ as sides and B as the vertex.
- $\mathcal{C}(O,r)$: the circle centered at O with radius r in the 2-D plane, thus $\mathcal{C}(O,r)=\{P\in\mathbb{R}^2|\ \|P-O\|_2=r\}$.
- $\mathcal{CV}(P_1,P_2)$: the connected curve in the 2-D plane with P_1 and P_2 as the two end points

A. Problem Formulation via Plane Geometry

The proposed approach is motivated by the crucial observation: the triangle in the m-dimensional Euclidean space with three sides given by $\|\mathbf{\Phi u}\|_2$, $\|\mathbf{\Phi v}\|_2$, and $\|\mathbf{\Phi}(\mathbf{u}-\mathbf{v})\|_2$ can be directly depicted in the 2-D plane (see Fig. 1). As a result, the study of the achievable angles between the two m-dimensional compressed vectors $\mathbf{\Phi u}$ and $\mathbf{\Phi v}$ can be formulated by means of such an auxiliary triangle from a plane geometry setting. In this way, the "algebraic"constraints (2.2), (2.3), and (2.7) can be jointly elucidated in a visualizable manner from a geometric perspective; more importantly, a joint analysis of these constraints within the plane geometry framework can, therefore, be carried out to derive closed-form solutions for $\alpha_{\max}$ and $\alpha_{\min}$, as will be seen later.

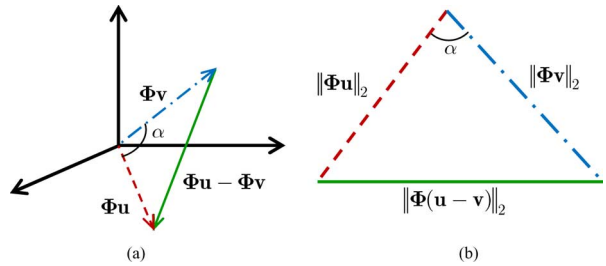

Fig. 1. (a) Triangle defined by the three m-dimensional vectors $\mathbf{\Phi u}$, $\mathbf{\Phi v}$, and $\mathbf{\Phi}(\mathbf{u}-\mathbf{v})$ (we use $m=3$ for illustration). (b) Depiction of the auxiliary triangle in the 2-D plane; in particular, based on the law of cosines (2.1), the angle α between $\mathbf{\Phi u}$ and $\mathbf{\Phi v}$ can be computed using $\|\mathbf{\Phi u}\|_2$, $\|\mathbf{\Phi v}\|_2$, and $\|\mathbf{\Phi}(\mathbf{u}-\mathbf{v})\|_2$.

To begin with, we shall leverage the idea of auxiliary triangles to translate the algebraic constraints (2.2), (2.3), and (2.7) into concrete geometric depictions in the 2-D plane. Toward this end, let us first pick a plausible compressed distance $\|\mathbf{\Phi}(\mathbf{u}-\mathbf{v})\|_2 = d$ such that $d_{\min}\le d\le d_{\max}$ [to meet constraint (2.3)] and construct all the feasible auxiliary triangles with a common bottom of length d. This can be done by drawing a line segment of length d, and then going on to find the locations of all feasible top vertices, whereof each one has the property that 1) the lengths of the two sides, i.e., $\|\mathbf{\Phi u}\|_2$ and $\|\mathbf{\Phi v}\|_2$, obey the norm constraint (2.2), and 2) the resultant $\|\mathbf{\Phi}(\mathbf{u}+\mathbf{v})\|_2^2$ satisfies (2.7).

Specifically, for a plausible d, let us draw a segment, say $\overline{B_dC_d}$, in the plane with $|\overline{B_dC_d}| = \|\mathbf{\Phi}(\mathbf{u}-\mathbf{v})\|_2 = d$ [see Fig. 2(a)]. We can first determine the region $\widehat{\mathbf{\Omega}}(d)$ such that, if $D_d\in\widehat{\mathbf{\Omega}}(d)$, then $|\overline{D_dB_d}| = \|\mathbf{\Phi u}\|_2$ and $|\overline{D_dC_d}| = \|\mathbf{\Phi v}\|_2$ fulfill (2.2), i.e., $\sqrt{1-\delta}\le|\overline{D_dB_d}|\le\sqrt{1+\delta}$ and $\sqrt{1-\delta}\le|\overline{D_dC_d}|\le\sqrt{1+\delta}$. For this, let us construct four circles, i.e., $\mathcal{C}(B_d,\sqrt{1+\delta})$, $\mathcal{C}(B_d,\sqrt{1-\delta})$, $\mathcal{C}(C_d,\sqrt{1+\delta})$, and $\mathcal{C}(C_d,\sqrt{1-\delta})$. Clearly, $\widehat{\mathbf{\Omega}}(d)$ is simply the intersection of the two annular regions defined by the four circles [5]; see the two gray regions in Fig. 2(a), and due to symmetry, it suffices to consider the one in the upper half. For a fixed $D_d\in\widehat{\mathbf{\Omega}}(d)$, the triangle $\Delta D_dB_dC_d$ is thus associated with the magnitude triple $(\|\mathbf{\Phi u}\|_2,\|\mathbf{\Phi v}\|_2,\|\mathbf{\Phi}(\mathbf{u}-\mathbf{v})\|_2) = (|\overline{D_dB_d}|,|\overline{D_dC_d}|,|\overline{B_dC_d}|=d)$, and the angle α between the m-dimensional vector pair $\{\mathbf{\Phi u},\mathbf{\Phi v}\}$ is exactly given by $\alpha=\measuredangle B_dD_dC_d$. Nevertheless, not every $D_d\in\widehat{\mathbf{\Omega}}(d)$ is feasible, since the corresponding $\|\mathbf{\Phi}(\mathbf{u}+\mathbf{v})\|_2^2$ may fail to satisfy the constraint (2.7). To further take (2.7) into account for identifying the locations of all feasible top vertices, we shall rewrite (2.7) in an alternative, yet equivalent, form more amenable to handle. For this, we first note that

$$\begin{aligned}\cos\alpha &= \frac{\langle\mathbf{\Phi u},\mathbf{\Phi v}\rangle}{\|\mathbf{\Phi u}\|_2\|\mathbf{\Phi v}\|_2}\\ &\overset{(a)}{=} \frac{\|\mathbf{\Phi u}+\mathbf{\Phi v}\|_2^2-\|\mathbf{\Phi u}-\mathbf{\Phi v}\|_2^2}{4\|\mathbf{\Phi u}\|_2\|\mathbf{\Phi v}\|_2}\\ &\overset{(b)}{=} \frac{\|\mathbf{\Phi u}+\mathbf{\Phi v}\|_2^2-d^2}{4\|\mathbf{\Phi u}\|_2\|\mathbf{\Phi v}\|_2} \quad (2.10)\end{aligned}$$

[5]The two annular regions defined by the four circles must overlap since, by invoking the definition of $d_{\max}$ in (2.4), it is easy to show that the sum of the radii of the two circles $\mathcal{C}(B_d,\sqrt{1+\delta})$ and $\mathcal{C}(C_d,\sqrt{1+\delta})$ is no less than d, that is, $\sqrt{1+\delta}+\sqrt{1+\delta}=2\sqrt{1+\delta}\ge d_{\max}\ge d=|\overline{B_dC_d}|$.

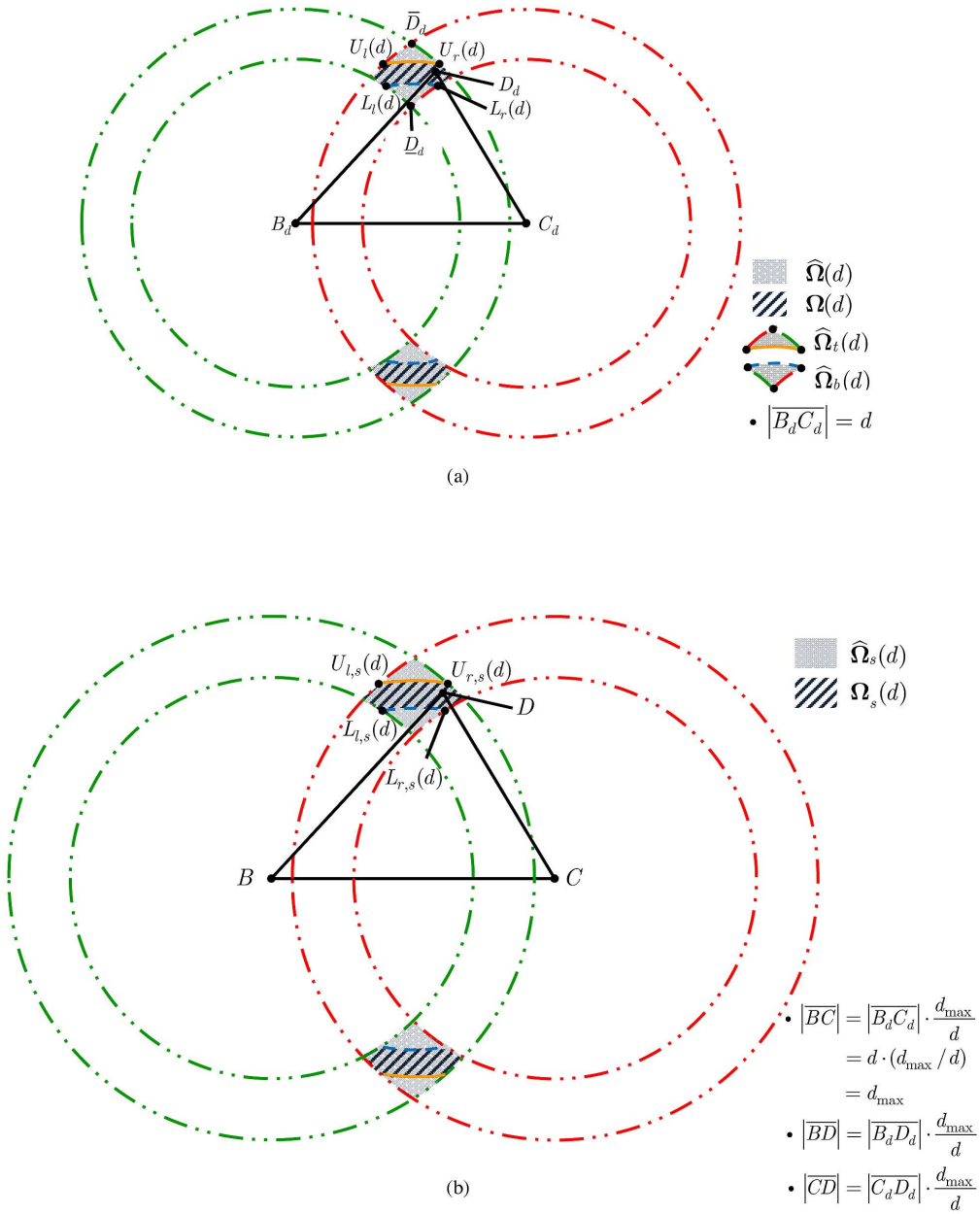

Fig. 2. (a) Schematic description of the feasible top-vertex set $\mathbf{\Omega}(d)$ associated with $\|\mathbf{\Phi}(\mathbf{u}-\mathbf{v})\|_2 = |\overline{B_dC_d}| = d$. (b) Dilation of (a) under the scale $d_{\max}/d$. The radius of each circle in (b) is $d_{\max}/(d)$ times the radius of the corresponding circle in (a). The dilated $\mathbf{\Omega}_s(d)$ is similar to $\mathbf{\Omega}(d)$. The dilated triangle ΔDBC in (b) is similar to $\Delta D_dB_dC_d$ in (a), thereby $\measuredangle D_dB_dC_d = \measuredangle DBC$.

where (a) follows from the polarization identity, and (b) holds since $\|\mathbf{\Phi}(\mathbf{u}-\mathbf{v})\|_2 = d$. Equation (2.10) then implies

$$\|\mathbf{\Phi}\mathbf{u}+\mathbf{\Phi}\mathbf{v}\|_2^2 = 4\,\|\mathbf{\Phi}\mathbf{u}\|_2\,\|\mathbf{\Phi}\mathbf{v}\|_2\cos\alpha + d^2. \tag{2.11}$$

By again invoking the law of cosines (2.1) and $\|\mathbf{\Phi}(\mathbf{u}-\mathbf{v})\|_2 = d$, we can rewrite (2.11) as

$$\begin{aligned}\|\mathbf{\Phi}\mathbf{u}+\mathbf{\Phi}\mathbf{v}\|_2^2 &= 2(\|\mathbf{\Phi}\mathbf{u}\|_2^2 + \|\mathbf{\Phi}\mathbf{v}\|_2^2) - d^2 \\ &= 2(|\overline{D_dB_d}|^2 + |\overline{D_dC_d}|^2) - d^2\end{aligned} \tag{2.12}$$

where the last equality holds since in our setting $\|\mathbf{\Phi}\mathbf{u}\|_2 = |\overline{D_dB_d}|$ and $\|\mathbf{\Phi}\mathbf{v}\|_2 = |\overline{D_dC_d}|$. Based on (2.12) together with some straightforward manipulations, the constraint (2.7) on $\|\mathbf{\Phi}(\mathbf{u}+\mathbf{v})\|_2^2$ can be equivalently rewritten in terms of $|\overline{D_dB_d}|^2 + |\overline{D_dC_d}|^2$ as follows:

$$\frac{\tilde{d}_{\min}^2 + d^2}{2} \le |\overline{D_dB_d}|^2 + |\overline{D_dC_d}|^2 \le \frac{\tilde{d}_{\max}^2 + d^2}{2}. \tag{2.13}$$

Hence, the feasible top-vertex set associated with $\|\mathbf{\Phi}(\mathbf{u}-\mathbf{v})\|_2 = |\overline{B_dC_d}| = d$, hereafter denoted by $\mathbf{\Omega}(d)$, consists of all $D_d \in \widehat{\mathbf{\Omega}}(d)$ that also satisfy (2.13), namely

$$\mathbf{\Omega}(d) = \left\{ D_d \;\middle|\; \begin{array}{l} D_d \in \widehat{\mathbf{\Omega}}(d), \\ \frac{\tilde{d}_{\min}^2+d^2}{2} \le |\overline{D_dB_d}|^2 + |\overline{D_dC_d}|^2 \le \frac{\tilde{d}_{\max}^2+d^2}{2} \end{array} \right\}. \tag{2.14}$$

From (2.14), it is easy to see that $\mathbf{\Omega}(d)$ can be obtained by removing from $\widehat{\mathbf{\Omega}}(d)$ the following two parts:

$$\widehat{\mathbf{\Omega}}_t(d)=\left\{D_d \,\middle|\, D_d\in\widehat{\mathbf{\Omega}}(d), |\overline{D_dB_d}|^2+|\overline{D_dC_d}|^2>\frac{\tilde{d}^2_{\max}+d^2}{2}\right\} \tag{2.15}$$

and

$$\widehat{\mathbf{\Omega}}_b(d)=\left\{D_d \,\middle|\, D_d\in\widehat{\mathbf{\Omega}}(d), |\overline{D_dB_d}|^2+|\overline{D_dC_d}|^2<\frac{\tilde{d}^2_{\min}+d^2}{2}\right\}. \tag{2.16}$$

Notably, $\widehat{\mathbf{\Omega}}_t(d)$ and $\widehat{\mathbf{\Omega}}_b(d)$, both in general nonempty,[6] represent the top and bottom "corner regions" of $\widehat{\mathbf{\Omega}}(d)$, respectively. The schematic depiction of $\mathbf{\Omega}(d)$ is, therefore, shown as the black-dashed region in Fig. 2(a); the top and bottom edges of $\mathbf{\Omega}(d)$ are characterized, respectively, by the two curves

$$\mathcal{CV}(U_l(d),U_r(d)) = \left\{D_d \,\middle|\, \begin{array}{l} D_d\in\mathbf{\Omega}(d),\\ |\overline{D_dB_d}|^2+|\overline{D_dC_d}|^2=(\tilde{d}^2_{\max}+d^2)/2\end{array}\right\} \tag{2.17}$$

and

$$\mathcal{CV}(L_l(d),L_r(d)) = \left\{D_d \,\middle|\, \begin{array}{l} D_d\in\mathbf{\Omega}(d),\\ |\overline{D_dB_d}|^2+|\overline{D_dC_d}|^2=(\tilde{d}^2_{\min}+d^2)/2\end{array}\right\}. \tag{2.18}$$

Associated with each $\|\mathbf{\Phi}(\mathbf{u}-\mathbf{v})\|_2 = d$ fulfilling (2.3), we have been able to specify the feasible top-vertex set $\mathbf{\Omega}(d)$. In particular, for $\mathbf{\Phi u}$ and $\mathbf{\Phi v}$ satisfying (2.2) and (2.7) subject to $\|\mathbf{\Phi}(\mathbf{u}-\mathbf{v})\|_2 = d$, the angle $\measuredangle(\mathbf{\Phi u},\mathbf{\Phi v})$ is exactly given by $\measuredangle(\mathbf{\Phi u},\mathbf{\Phi v})=\measuredangle B_dD_dC_d$ for some $D_d\in\mathbf{\Omega}(d)$; hence, we have

$$\left\{\measuredangle(\mathbf{\Phi u},\mathbf{\Phi v})\,\middle|\, \begin{array}{l}\mathbf{\Phi u} \text{ and } \mathbf{\Phi v} \text{ satisfy (2.2)}\\ \text{and (2.7) subject to } \|\mathbf{\Phi}(\mathbf{u}-\mathbf{v})\|_2=d\end{array}\right\} = \left\{\measuredangle B_dD_dC_d \,\middle|\, D_d\in\mathbf{\Omega}(d), |\overline{B_dC_d}|=d\right\}. \tag{2.19}$$

The significance of such a formulation is that all the considered norm/distance constraints imposed by RIP can be jointly characterized via simple and visualizable geometric depictions in the 2-D plane. Based on the above plane geometry framework, the proposed approach for the identification of $\alpha_{\max}$ and $\alpha_{\min}$ is shown next.

B. Proposed Approach via Similarity

Given a plausible d and the corresponding $\mathbf{\Omega}(d)$ constructed as above, one may immediately proceed to seek among all $D_d\in\mathbf{\Omega}(d)$ to find

$$\alpha_{\max}(d)=\max_{D_d\in\mathbf{\Omega}(d)}\measuredangle B_dD_dC_d$$

and

$$\alpha_{\min}(d)=\min_{D_d\in\mathbf{\Omega}(d)}\measuredangle B_dD_dC_d$$

associated with the particular d. Once $\alpha_{\max}(d)$'s and $\alpha_{\min}(d)$'s for all feasible d are obtained, the maximal and minimal α can be determined as

$$\alpha_{\max}=\max_{d_{\min}\le d\le d_{\max}}\alpha_{\max}(d)$$

and

$$\alpha_{\min}=\min_{d_{\min}\le d\le d_{\max}}\alpha_{\min}(d).$$

Such a method, even though conceptually simple, is nonetheless a daunting task since there are uncountably many candidate d. This thus motivates us to devise afresh an alternative free of the aforementioned drawbacks. Ideally, if we can come up with a *single* diagram tractably depicting *all* feasible auxiliary triangles $\Delta D_dB_dC_d$ associated with *all* compressed distances $d_{\min}\le d\le d_{\max}$, it only remains to consider such a diagram for the identification of $\alpha_{\max}$ and $\alpha_{\min}$. To realize this idea, we resort to the technique of *similarity* in the plane geometry analysis.

Definition 2.1 [29]: Two figures in the plane are similar whenever one is congruent to a dilation of the other. □

A well-known result is that if two polygons are similar, the corresponding sides are in proportion and the corresponding angles must be equal (the so-called conformal property) [30]. Now, suppose we have a figure similar to Fig. 2(a). For each $\Delta D_dB_dC_d$, there is one and only one corresponding triangle, say, ΔDBC, in the similar figure, and $\Delta D_dB_dC_d$ is similar to ΔDBC. Thanks to the conformal property, it follows $\measuredangle B_dD_dC_d=\measuredangle BDC$. Given this fact, we can instead focus on the similar figure as far as the characterization of achievable $\measuredangle B_dD_dC_d$ is concerned. With the aid of judiciously constructed similar figures for all $d_{\min}\le d\le d_{\max}$, there is a simple way to obtain a single diagram depicting *all* the similar feasible auxiliary triangles ΔDBC. Therefore, a unified and tractable plane geometry analysis can be conducted to identify $\alpha_{\max}$ and $\alpha_{\min}$.

To proceed, let us first highlight the main idea about the construction of the desired single diagram. Recall from Fig. 2(a) that, for a plausible d, all the associated feasible auxiliary triangles $\Delta D_dB_dC_d$'s are with a bottom of length d. In other words, for any two sets of such triangles associated with two plausible $d_1\neq d_2$, the corresponding bottoms assume different lengths: this makes it difficult to "merge" all the auxiliary triangles for all $d_{\min}\le d\le d_{\max}$ into a single diagram. To rid this difficulty, one intuitive approach is to come up with alternative sets of triangles, which have the properties that 1) the bottoms of all the triangles are with equal length, regardless of the values of d, and 2) the set of measures of all angles defined by the top vertexes remain identical to $\{\measuredangle B_dD_dC_d | D_d\in\mathbf{\Omega}(d), d_{\min}\le d\le d_{\max}\}$. Now, the idea of similarity comes into play. Specifically, for

[6] $\widehat{\mathbf{\Omega}}_t(d)$ contains the point $\bar{D}_d$, the intersection of the two circles $\mathcal{C}(B_d,\sqrt{1+\delta})$ and $\mathcal{C}(C_d,\sqrt{1+\delta})$, unless $d=d_{\max}$. This is because $|\overline{\bar{D}_dB_d}|^2+|\overline{\bar{D}_dC_d}|^2=2(1+\delta)\overset{(a)}{=}(\tilde{d}^2_{\max}+d^2_{\max})/2\overset{(b)}{\ge}(\tilde{d}^2_{\max}+d^2)/2$, where (a) follows from (2.4) and (2.8), and (b) holds since $d_{\max}\ge d$; inequality (b) becomes equality when $d=d_{\max}$. In an analogous way, it can be verified that $\widehat{\mathbf{\Omega}}_b(d)$ contains $\underline{D}_d$, the intersection of $\mathcal{C}(B_d,\sqrt{1-\delta})$ and $\mathcal{C}(C_d,\sqrt{1-\delta})$, and is thus nonempty (unless $d=d_{\min}$).

each d, we will first obtain a figure similar to Fig. 2(a) via a dilation with the scale $\frac{d_{\max}}{d}$ (≥ 1). Let ΔDBC be the dilated version of $\Delta D_dB_dC_d$, for $D_d \in \mathbf{\Omega}(d)$, in the similar figure. Thus, ΔDBC is similar to $\Delta D_dB_dC_d$ (accordingly, $\measuredangle B_dD_dC_d = \measuredangle BDC$) and, moreover, $|\overline{BC}| = |\overline{B_dC_d}| \cdot \frac{d_{\max}}{d} = d \cdot \frac{d_{\max}}{d} = d_{\max}$, meaning that the bottom-length of each similar auxiliary triangle is then fixed to $d_{\max}$, no matter what the value of d is. Such an equal bottom-length characteristic then allows for a simple way of depicting all similar auxiliary triangles on a single diagram.

The construction of such a diagram based on the aforementioned approach involves two steps as detailed below.

(I) *Construction of the Similar Figure Associated with a Plausible d*: For a plausible compressed distance $\|\mathbf{\Phi}(\mathbf{u}-\mathbf{v})\|_2 = |\overline{B_dC_d}| = d$, let us uniformly stretch all geometric objects in Fig. 2(a) by the scale $\frac{d_{\max}}{d}$ (≥ 1) to obtain the dilated similar figure as depicted in Fig. 2(b), in which $\mathbf{\Omega}_s(d)$ is similar to $\mathbf{\Omega}(d)$ and, for each $D_d \in \mathbf{\Omega}(d)$, there exists one and only one corresponding $D \in \mathbf{\Omega}_s(d)$ such that $|\overline{BD}| = \frac{d_{\max}}{d} \cdot |\overline{B_dD_d}|$, $|\overline{CD}| = \frac{d_{\max}}{d} \cdot |\overline{C_dD_d}|$, and $|\overline{BC}| = \frac{d_{\max}}{d} \cdot |\overline{B_dC_d}| = \frac{d_{\max}}{d} \cdot d = d_{\max}$, and therefore, ΔDBC in Fig. 2(b) is similar to $\Delta D_dB_dC_d$ in Fig. 2(a). The conformal characteristic of similarity asserts $\measuredangle B_dD_dC_d = \measuredangle BDC$; thus

$$\left\{\measuredangle B_dD_dC_d \middle| D_d \in \mathbf{\Omega}(d), |\overline{B_dC_d}| = d\right\} = \left\{\measuredangle BDC \middle| D \in \mathbf{\Omega}_s(d), |\overline{BC}| = d_{\max}\right\}. \quad (2.20)$$

Notably, through the proposed dilation procedure, the length of the enlarged $\|\mathbf{\Phi}(\mathbf{u}-\mathbf{v})\|_2 = |\overline{B_dC_d}|$ is then *fixed* to be $d \cdot \frac{d_{\max}}{d} = d_{\max}$ irrespective of d. That is to say, *all* the similar auxiliary triangles associated with *all* plausible d's are with bottoms of identical length, equal to $d_{\max}$.

Specific procedures for constructing the similar figure for a plausible d as mentioned above are as follows.

(a) Draw the line segment $\overline{BC}$ with $|\overline{BC}| = d_{\max}$.

(b) Obtain $\widehat{\mathbf{\Omega}}_s(d)$ the dilation of $\widehat{\mathbf{\Omega}}(d)$ in Fig. 2(a), as the intersection of the annular region defined by the four enlarged circles $\mathcal{C}(B, \sqrt{1+\delta} \cdot (d_{\max}/d))$, $\mathcal{C}(B, \sqrt{1-\delta} \cdot (d_{\max}/d))$, $\mathcal{C}(C, \sqrt{1+\delta} \cdot (d_{\max}/d))$ and $\mathcal{C}(C, \sqrt{1-\delta} \cdot (d_{\max}/d))$.

(c) Determine $\mathbf{\Omega}_s(d)$ by specifying its top and bottom edges, which are the dilations of, respectively, $\mathcal{CV}(U_l(d), U_r(d))$ in (2.17) and $\mathcal{CV}(L_l(d), L_r(d))$ in (2.18). For this, we note that, if $\overline{DB}$ and $\overline{DC}$ associated with $D \in \mathbf{\Omega}_s(d)$ are, respectively, the dilated $\overline{D_dB_d}$ and $\overline{D_dC_d}$, where $D_d \in \mathbf{\Omega}(d)$, it immediately follows that $|\overline{DB}|^2 = (\frac{d_{\max}}{d})^2 \cdot |\overline{D_dB_d}|^2$ and $|\overline{DC}|^2 = (\frac{d_{\max}}{d})^2 \cdot |\overline{D_dB_d}|^2$ With this fact in mind, the dilated top and bottom edges can be accordingly determined from (2.17) and (2.18) as, respectively, (2.21) and (2.22) at the bottom of the page.

(II) *Depiction of all Similar Feasible Auxiliary Triangles in one Diagram*: Now, each similar auxiliary triangle ΔDBC, where $D \in \mathbf{\Omega}_s(d)$, for any $d_{\min} \leq d \leq d_{\max}$, is with a common bottom-length $d_{\max}$. The identical bottom-length property suggests that we can place all ΔDBC "one on the top of another" in the plane, with all bottoms aligned altogether, to obtain the desired single diagram. Equivalently, this can be done via first drawing a line segment of length $d_{\max}$ as the common bottom, followed by locating the topic vertexes of all similar auxiliary triangles, namely, $D \in \mathbf{\Omega}_s(d)$ for all $d_{\min} \leq d \leq d_{\max}$, in the plane. The procedures are as follows:

(d) Draw the common referenced line segment $\overline{BC}$ with $|\overline{BC}| = d_{\max}$.

(e) Repeatedly use steps (b) and (c) in part (I) to construct $\mathbf{\Omega}_s(d)$'s for all $d_{\min} \leq d \leq d_{\max}$.

Observe that, as d decreases from $d_{\max}$ to $d_{\min}$, the radii of the four circles constructed in step (b) will increase, and so do $\gamma_t(d)$ in (2.21) and $\gamma_b(d)$ in (2.22). Hence, as d decreases, the intersection of the annular region defined by the four circles, as well as the dilated top and bottom edges in (2.21) and (2.22), is "pushed away" from $\overline{BC}$: this implies that $\mathbf{\Omega}_s(d)$ constructed by (e) continuously "moves upward" as d decreases from $d_{\max}$ to $d_{\min}$ (see Fig. 3). The joint feasible top-vertex set $\mathbf{\Omega}$, which consists of the top vertexes of all similar auxiliary triangles with $\overline{BC}$ as the common bottom, is obtained as the union of all $\mathbf{\Omega}_s(d)$'s, namely,

$$\mathbf{\Omega} = \bigcup_{d_{\min} \leq d \leq d_{\max}} \mathbf{\Omega}_s(d). \quad (2.23)$$

$$\mathcal{CV}(U_{l,s}(d), U_{r,s}(d)) = \left\{ D \middle| D \in \mathbf{\Omega}_s(d), |\overline{DB}|^2 + |\overline{DC}|^2 = \frac{\tilde{d}_{\max}^2 + d^2}{2} \cdot \left(\frac{d_{\max}^2}{d^2}\right) = \underbrace{\frac{\tilde{d}_{\max}^2(d_{\max}^2/d^2) + d_{\max}^2}{2}}_{:=\gamma_t(d)} \right\} \quad (2.21)$$

$$\mathcal{CV}(L_{l,s}(d), L_{r,s}(d)) = \left\{ D \middle| D \in \mathbf{\Omega}_s(d), |\overline{DB}|^2 + |\overline{DC}|^2 = \frac{\tilde{d}_{\min}^2 + d^2}{2} \cdot \left(\frac{d_{\max}^2}{d^2}\right) = \underbrace{\frac{\tilde{d}_{\min}^2(d_{\max}^2/d^2) + d_{\max}^2}{2}}_{:=\gamma_b(d)} \right\} \quad (2.22)$$

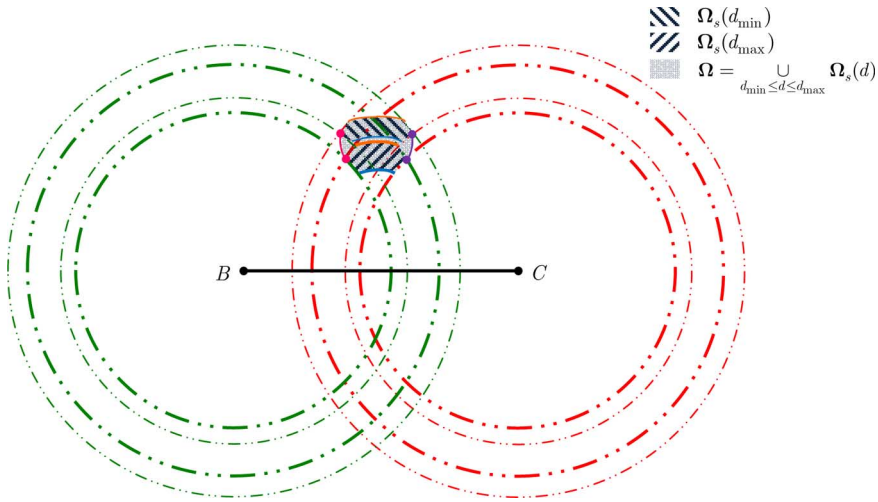

Fig. 3. Schematic description of the joint feasible top-vertex set $\mathbf{\Omega}$.

Note that, in the 2-D plane, $\mathbf{\Omega}$ is the collection of the overlaid $\mathbf{\Omega}_s(d)$'s, with $\mathbf{\Omega}_s(d_{\min})$ on the top and $\mathbf{\Omega}_s(d_{\max})$ at the bottom. The depiction of $\mathbf{\Omega}$ is shown as the gray part in Fig. 3. As a result, each similar feasible auxiliary triangle can be depicted in Fig. 3 as ΔDBC for some $D \in \mathbf{\Omega}$, thereby

$$\bigcup_{d_{\min}\le d\le d_{\max}} \left\{ \measuredangle BDC \middle| D \in \mathbf{\Omega}_s(d) \right\} = \left\{ \measuredangle BDC \middle| D \in \mathbf{\Omega} \right\}. \tag{2.24}$$

Now, we can reach the following conclusions:

$$\begin{aligned} &\left\{ \measuredangle(\mathbf{\Phi u}, \mathbf{\Phi v}) \middle| \mathbf{\Phi u} \text{ and } \mathbf{\Phi v} \text{ satisfy (2.2), (2.3), and (2.7)} \right\} \\ &\overset{(a)}{=} \bigcup_{d_{\min}\le d\le d_{\max}} \left\{ \measuredangle B_d D_d C_d \middle| D_d \in \mathbf{\Omega}(d), |\overline{B_d C_d}| = d \right\} \\ &\overset{(b)}{=} \bigcup_{d_{\min}\le d\le d_{\max}} \left\{ \measuredangle BDC \middle| D \in \mathbf{\Omega}_s(d), |\overline{BC}| = d_{\max} \right\} \\ &\overset{(c)}{=} \left\{ \measuredangle BDC \middle| D \in \mathbf{\Omega} \right\} \end{aligned} \tag{2.25}$$

where (a) can be directly inferred from (2.19), (b) follows from (2.20), and (c) holds due to (2.24). The result of (2.25) then leads to the key theorem given below.

Theorem 2.2: The following result holds:

$$\alpha_{\max} = \max_{D\in\mathbf{\Omega}} \measuredangle BDC \text{ and } \alpha_{\min} = \min_{D\in\mathbf{\Omega}} \measuredangle BDC. \tag{2.26}$$

□

Theorem 2.2 provides the foundation behind the proposed approach. In particular, (2.26) asserts that we can focus on the single diagram as Fig. 3, based on which plane geometry analyses can be then conducted to identify $\alpha_{\max}$ and $\alpha_{\min}$.

C. Further Characterization of the Joint Feasible Top-Vertex Set $\mathbf{\Omega}$

According to Theorem 2.2, all we have to do is to seek among all $D \in \mathbf{\Omega}$ for the two that will, respectively, yield the maximal and minimal $\measuredangle BDC$ [cf., (2.26)]. Intuitively speaking, $\alpha_{\max}$ and $\alpha_{\min}$ are very likely to be attained by some points located on

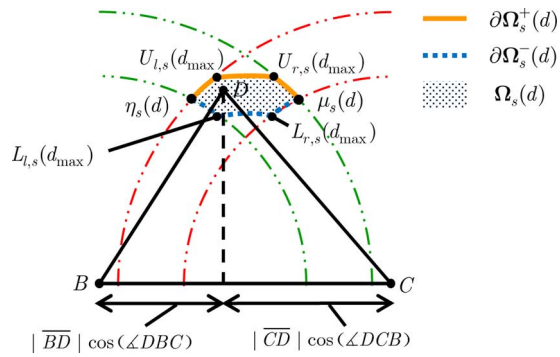

Fig. 4. Decomposition of the boundary $\partial\mathbf{\Omega}_s(d)$ as the connection of $\partial\mathbf{\Omega}_s^+(d)$ and $\partial\mathbf{\Omega}_s^-(d)$.

$\partial\mathbf{\Omega}$, the boundary of $\mathbf{\Omega}$. By conducting plane geometry analyses based on the diagram in Fig. 3, such a simple idea turns out to be true, as will be shown below. The result allows us to further narrow down the candidate top vertices in $\mathbf{\Omega}$ so as to simplify the identification of $\alpha_{\max}$ and $\alpha_{\min}$.

To proceed, we shall first provide more concrete characterization of $\partial\mathbf{\Omega}$; in particular, the left, right, top, and bottom components of $\partial\mathbf{\Omega}$ will be specified. For this, associated with each similar feasible top-vertex set $\mathbf{\Omega}_s(d)$, we define

$$\begin{aligned} \eta_s(d) &\overset{\triangle}{=} \arg\min_{D\in\mathbf{\Omega}_s(d)} |\overline{BD}| \cos(\measuredangle DBC) \\ \mu_s(d) &\overset{\triangle}{=} \arg\min_{D\in\mathbf{\Omega}_s(d)} |\overline{CD}| \cos(\measuredangle DCB). \end{aligned} \tag{2.27}$$

Here, $\eta_s(d)$ and $\mu_s(d)$ represent, respectively, the left and right corner points of $\mathbf{\Omega}_s(d)$ (see Fig. 4). Let us then decompose the boundary of $\mathbf{\Omega}_s(d)$, say $\partial\mathbf{\Omega}_s(d)$, into the connection of two branches as

$$\partial\mathbf{\Omega}_s(d) = \partial\mathbf{\Omega}_s^+(d) \cup \mathbf{\Omega}_s^-(d) \tag{2.28}$$

where $\partial\mathbf{\Omega}_s^+(d)$ and $\partial\mathbf{\Omega}_s^-(d)$ are, respectively, the upper and lower branches both with $\eta_s(d)$ and $\mu_s(d)$ as the end points (see Fig. 4). Since $\mathbf{\Omega}$ is obtained by overlaying all the continuum $\mathbf{\Omega}_s(d)$'s, with $\mathbf{\Omega}_s(d_{\min})$ on the top and $\mathbf{\Omega}_s(d_{\max})$ at the bottom

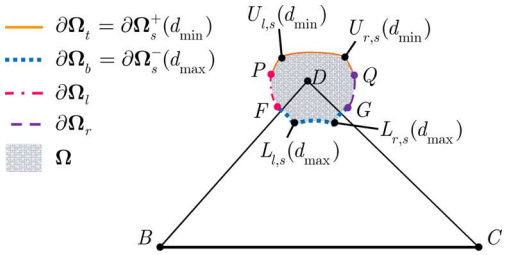

Fig. 5. Depiction of the boundary of $\mathbf{\Omega}$, in which $\partial\mathbf{\Omega}_t$, $\partial\mathbf{\Omega}_b$, $\partial\mathbf{\Omega}_l$, and $\partial\mathbf{\Omega}_r$ are, respectively, the top, bottom, left, and right boundaries.

(recall the construction of $\mathbf{\Omega}$), the upper branch of $\mathbf{\Omega}_s(d_{\min})$ and the lower branch of $\mathbf{\Omega}_s(d_{\max})$ must belong to $\partial\mathbf{\Omega}$, i.e., $\partial\mathbf{\Omega}_s^+(d_{\min}) \subset \partial\mathbf{\Omega}$ and $\partial\mathbf{\Omega}_s^-(d_{\max}) \subset \partial\mathbf{\Omega}$. This naturally suggests that the top and bottom boundaries of $\mathbf{\Omega}$, denoted by $\partial\mathbf{\Omega}_t$ and $\partial\mathbf{\Omega}_b$, can be specified, respectively, as

$$\partial\mathbf{\Omega}_t = \partial\mathbf{\Omega}_s^+(d_{\min}) \tag{2.29}$$

and

$$\partial\mathbf{\Omega}_b = \partial\mathbf{\Omega}_s^-(d_{\max}). \tag{2.30}$$

With $\partial\mathbf{\Omega}_t$ and $\partial\mathbf{\Omega}_b$ given as above, we can go on to determine the left and right boundaries of $\mathbf{\Omega}$, denoted by $\partial\mathbf{\Omega}_l$ and $\partial\mathbf{\Omega}_r$ respectively. Indeed, $\partial\mathbf{\Omega}_l$ is simply the boundary curve with end points $\eta_s(d_{\min})$ and $\eta_s(d_{\max})$, namely, the left ends of $\partial\mathbf{\Omega}_t$ and $\partial\mathbf{\Omega}_b$; similarly, $\partial\mathbf{\Omega}_r$ is the portion with $\mu_s(d_{\min})$ and $\mu_s(d_{\max})$ as the two ends. Note that by construction of $\mathbf{\Omega}$, it follows

$$\begin{aligned}\partial\mathbf{\Omega}_l =& \{\eta_s(d) | d_{\min} \le d \le d_{\max}\} \\ \partial\mathbf{\Omega}_r =& \{\mu_s(d) | d_{\min} \le d \le d_{\max}\}\end{aligned} \tag{2.31}$$

which are the collections of, respectively, the left and right corner points of $\mathbf{\Omega}_s(d)$ for all plausible d. Hence, we have $\partial\mathbf{\Omega} = \partial\mathbf{\Omega}_r \cup \partial\mathbf{\Omega}_l \cup \partial\mathbf{\Omega}_t \cup \partial\mathbf{\Omega}_b$; see Fig. 5 for the depiction of the four boundary components, and in the sequel, we use the shorthand (P, Q, F, G) to denote the four end points $(\eta_s(d_{\min}), \mu_s(d_{\min}), \eta_s(d_{\max}), \mu_s(d_{\max}))$ in order to conserve notation. With the above characterizations of $\partial\mathbf{\Omega}$, the main result of this section is then given in the next theorem, which asserts that the candidate top vertices relevant to the identification of $\alpha_{\max}$ and $\alpha_{\min}$ can be narrowed down to those on, respectively, $\partial\mathbf{\Omega}_b$ and $\partial\mathbf{\Omega}_t$.

Theorem 2.3: $\alpha_{\max} = \measuredangle BDC$ for some $D \in \partial\mathbf{\Omega}_b$, and $\alpha_{\min} = \measuredangle BD'C$ for some $D' \in \partial\mathbf{\Omega}_t$.

Proof: See Appendix A. □

Based on the established results, the derivations of $\alpha_{\max}$ and $\alpha_{\min}$ are given in Sections III and IV.

III. Derivation of $\alpha_{\max}$

In this section, we will conduct plane geometry analyses based on Fig. 5 to derive $\alpha_{\max}$. According to Theorem 2.3 and (2.30), our task is to find the largest $\measuredangle BDC$ among all $D \in \partial\mathbf{\Omega}_s^-(d_{\max})$, which is the lower branch of $\mathbf{\Omega}_s(d_{\max})$. It is worth mentioning that all the feasible auxiliary triangles are with a common bottom $\overline{BC}$ with $|\overline{BC}| = d_{\max}$, and $\partial\mathbf{\Omega}_s^-(d_{\max})$ is depicted as a connected curve in the 2-D plane. To seek for the maximal $\measuredangle BDC$ for $D \in \partial\mathbf{\Omega}_s^-(d_{\max})$, the underlying approach lies in first constructing certain auxiliary circles, with $\overline{BC}$ as a chord, on the plane. Then, by exploiting the location of points on $\partial\mathbf{\Omega}_s^-(d_{\max})$ relative to the auxiliary circles, together with various properties regarding the inscribed angles that are well established in the plane geometry context, plane geometry analyses are conducted to find the solution (details referred to the appendix). The main results of this section are established in Theorems 3.2 and 3.4.

To proceed, we shall first highlight the main idea behind the proof. Let us decompose $\partial\mathbf{\Omega}_s^-(d_{\max})$ as the union of three boundary curves $\mathcal{CV}(F, L_{l,s}(d_{\max}))$, $\mathcal{CV}(L_{l,s}(d_{\max}), L_{r,s}(d_{\max}))$, and $\mathcal{CV}(L_{r,s}(d_{\max}), G)$ as shown in Fig. 5. We propose to first find the maximal $\measuredangle BDC$ for $D \in \mathcal{CV}(L_{l,s}(d_{\max}), L_{r,s}(d_{\max}))$. The main advantages of such an approach are twofold. First, the cosine of $\measuredangle BDC$ for $D \in \mathcal{CV}(L_{l,s}(d_{\max}), L_{r,s}(d_{\max}))$, as will be shown later, admits a very simple expression in terms of $|\overline{DB}|$ and $|\overline{DC}|$. With the aid of this expression, finding the maximal $\measuredangle BDC$ for $D \in \mathcal{CV}(L_{l,s}(d_{\max}), L_{r,s}(d_{\max}))$ can be mathematically formulated as a constrained optimization problem which is analytically solvable. Second, even though the feasible set of such an optimization problem consists of only those $D \in \mathcal{CV}(L_{l,s}(d_{\max}), L_{r,s}(d_{\max}))$, the solution to this problem can act as a yardstick point, to which the achievable $\measuredangle BDC$ for all $D \in \mathcal{CV}(F, L_{l,s}(d_{\max})) \cup \mathcal{CV}(L_{l,s}(d_{\max}), L_{r,s}(d_{\max})) \cup \mathcal{CV}(L_{r,s}(d_{\max}), G)$ can be readily compared via plane geometry analyses: this thus provides a unified and systematic way of identifying $\alpha_{\max}$.

Since by construction, $\mathcal{CV}(L_{l,s}(d_{\max}), L_{r,s}(d_{\max}))$ is the bottom edge of $\mathbf{\Omega}_s(d_{\max})$ (see Fig. 2(b) with $d = d_{\max}$), for any $D \in \mathcal{CV}(L_{l,s}(d_{\max}), L_{r,s}(d_{\max}))$, the sum of the squared length $|\overline{DB}|^2 + |\overline{DC}|^2$ must satisfy [cf., (2.22)]

$$\begin{aligned}|\overline{DB}|^2 + |\overline{DC}|^2 &= \left\{ \frac{(\tilde{d}_{\min}^2 (d_{\max}/d)^2 + d_{\max}^2)}{2} \right\}_{d=d_{\max}} \\ &= \frac{\tilde{d}_{\min}^2 + d_{\max}^2}{2}.\end{aligned} \tag{3.1}$$

With (3.1) and since $|\overline{BC}| = d_{\max}$, we have

$$\begin{aligned}\cos(\measuredangle BDC) &= \frac{|\overline{DB}|^2 + |\overline{DC}|^2 - |\overline{BC}|^2}{2|\overline{DB}| \cdot |\overline{DC}|} \\ &= \frac{\frac{\tilde{d}_{\min}^2 + d_{\max}^2}{2} - d_{\max}^2}{2|\overline{DB}| \cdot |\overline{DC}|} \\ &= \frac{\tilde{d}_{\min}^2 - d_{\max}^2}{4|\overline{DB}| \cdot |\overline{DC}|}.\end{aligned} \tag{3.2}$$

Hence, for $D \in \mathcal{CV}(L_{l,s}(d_{\max}), L_{r,s}(d_{\max}))$, $\cos(\measuredangle BDC)$ depends on $\tilde{d}_{\min}^2 - d_{\max}^2$ as well as the product length $|\overline{DB}| \cdot |\overline{DC}|$. Since $\tilde{d}_{\min}^2 - d_{\max}^2$ is a constant independent of the top vertex D [see (2.4) and (2.9)], to simplify the exposure we proceed to find the maximal $\measuredangle BDC$, or the minimal $\cos(\measuredangle BDC)$, by first considering the scenario $\tilde{d}_{\min}^2 - d_{\max}^2 \ge 0$.

A. Case I: $\tilde{d}^2_{\min} - d^2_{\max} \geq 0$

Since $\tilde{d}^2_{\min} - d^2_{\max} \geq 0$, (3.2) shows that minimization of $\cos(\measuredangle BDC)$ amounts to maximizing the product $|\overline{DB}| \cdot |\overline{DC}|$. Observe that

$$\left(|\overline{DB}| + |\overline{DC}|\right)^2 = |\overline{DB}|^2 + |\overline{DC}|^2 + 2|\overline{DB}| \cdot |\overline{DC}| \overset{(a)}{=} \frac{\tilde{d}^2_{\min} + d^2_{\max}}{2} + 2|\overline{DB}| \cdot |\overline{DC}| \quad (3.3)$$

where (a) follows from (3.1). Equation (3.3) implies that, to maximize $|\overline{DB}| \cdot |\overline{DC}|$, it is equivalent to maximize the summed length $|\overline{DB}| + |\overline{DC}|$. As a result, minimization of $\cos(\measuredangle BDC)$ among all $D \in \mathcal{CV}(L_{l,s}(d_{\max}), L_{r,s}(d_{\max}))$ under the case $\tilde{d}^2_{\min} - d^2_{\max} \geq 0$ can be formulated as a constrained optimization problem as

$$(P1) \quad Maximize\ |\overline{DB}| + |\overline{DC}|, \quad subject\ to \begin{cases} (i)\ |\overline{DB}|^2 + |\overline{DC}|^2 = (\tilde{d}^2_{\min} + d^2_{\max})/2, \\ (ii)\ \sqrt{1-\delta} \leq |\overline{DB}| \leq \sqrt{1+\delta}, \\ (iii) \sqrt{1-\delta} \leq |\overline{DC}| \leq \sqrt{1+\delta}. \end{cases}$$

Note that the three constraints in $(P1)$ are indeed the characterization of $|\overline{DB}|$ and $|\overline{DC}|$ for $D \in \mathcal{CV}(L_{l,s}(d_{\max}), L_{r,s}(d_{\max}))$ [cf., (2.22)]. The optimal D obtained by solving the above optimization problem is given in the next lemma.

Lemma 3.1: Let $d^2_{\max}$ and $\tilde{d}^2_{\min}$ be defined in, respectively, (2.4) and (2.9). If $\tilde{d}^2_{\min} - d^2_{\max} \geq 0$, and let $D_L \in \mathcal{CV}(L_{l,s}(d_{\max}), L_{r,s}(d_{\max}))$ be such that

$$|\overline{D_L B}| = |\overline{D_L C}| = \sqrt{(\tilde{d}^2_{\min} + d^2_{\max})/4} \quad (3.4)$$

then the optimal $(|\overline{DB}|, |\overline{DC}|)$ which solves (P1) is uniquely given by $(|\overline{D_L B}|, |\overline{D_L C}|)$.

Proof: See Appendix B. □

As a result of Lemma 3.1, we have $\measuredangle BD_L C > \measuredangle BDC$ for all $D \in \mathcal{CV}(L_{l,s}(d_{\max}), L_{r,s}(d_{\max})) \backslash \{D_L\}$. Roughly speaking, the closer the top vertex D is to the bottom $\overline{BC}$, the larger the angle $\measuredangle BDC$ will be. Since among the three boundary curves $\mathcal{CV}(F, L_{r,s}(d_{\max}))$, $\mathcal{CV}(L_{l,s}(d_{\max}), L_{r,s}(d_{\max}))$, and $\mathcal{CV}(L_{l,s}(d_{\max}), G)$, the second one, namely, $\mathcal{CV}(L_{l,s}(d_{\max}), L_{r,s}(d_{\max}))$, is located nearer to $\overline{BC}$ (see Fig. 5), it is expected that the maximally achievable $\measuredangle BDC$ for $D \in \mathcal{CV}(L_{l,s}(d_{\max}), L_{r,s}(d_{\max}))$, namely, $\measuredangle BD_L C$, is the global $\alpha_{\max}$. This turns out to be true, as shown in the following theorem.

Theorem 3.2: Let $d^2_{\max}$ and $\tilde{d}^2_{\min}$ be defined in, respectively, (2.4) and (2.9). If $\tilde{d}^2_{\min} - d^2_{\max} \geq 0$, we have

$$\alpha_{\max} = \measuredangle BD_L C = \cos^{-1}\left(\frac{\tilde{d}^2_{\min} - d^2_{\max}}{\tilde{d}^2_{\min} + d^2_{\max}}\right). \quad (3.5)$$

Proof: See Appendix C. □

B. Case II: $\tilde{d}^2_{\min} - d^2_{\max} < 0$

Based on (3.2), it can be readily seen that, with $\tilde{d}^2_{\min} - d^2_{\max} < 0$, minimization of $\cos(\measuredangle BDC)$ thus amounts to minimizing (instead of maximizing) the denominator $|\overline{DB}| \cdot |\overline{DC}|$. With the aid of (3.3), this is then equivalent to minimize the summed length $|\overline{DB}| + |\overline{DC}|$. Specifically, the maximal $\measuredangle BDC$ for all $D \in \mathcal{CV}(L_{l,s}(d_{\max}), L_{r,s}(d_{\max}))$ in this case can be obtained as the solution to the following constrained optimization problem

$$(P2) \quad Minimize\ |\overline{DB}| + |\overline{DC}|, \quad subject\ to \begin{cases} (i)\ |\overline{DB}|^2 + |\overline{DC}|^2 = (\tilde{d}^2_{\min} + d^2_{\max})/2, \\ (ii)\ \sqrt{1-\delta} \leq |\overline{DB}| \leq \sqrt{1+\delta}, \\ (iii) \sqrt{1-\delta} \leq |\overline{DC}| \leq \sqrt{1+\delta}. \end{cases}$$

The optimal solution obtained by solving $(P2)$ is given in the next lemma.

Lemma 3.3: Let $d^2_{\max}$ and $\tilde{d}^2_{\min}$ be defined in, respectively, (2.4) and (2.9). If $\tilde{d}^2_{\min} - d^2_{\max} < 0$, the optimal $(|\overline{DB}|, |\overline{DC}|)$ which solves (P2) is given by $(|\overline{L_{l,s}(d_{\max})B}|, |\overline{L_{l,s}(d_{\max})C}|)$ or $(|\overline{L_{r,s}(d_{\max})B}|, |\overline{L_{r,s}(d_{\max})C}|)$.

Proof: See Appendix D. □

From Lemma 3.3, it follows that the maximal $\measuredangle BDC$ among all $D \in \mathcal{CV}(L_{l,s}(d_{\max}), L_{r,s}(d_{\max}))$ is attained by $D = L_{l,s}(d_{\max})$ or $D = L_{r,s}(d_{\max})$. Through further plane geometry analyses, the maximal angle in this case is derived in the next theorem.

Theorem 3.4: Let $d^2_{\max}$ and $\tilde{d}^2_{\min}$ be defined in, respectively, (2.4) and (2.9). If $\tilde{d}^2_{\min} - d^2_{\max} < 0$, the following results hold.

1) If $\tilde{d}^2_{\min} + d^2_{\max} \leq 4$, then

$$\alpha_{\max} = \cos^{-1}\left\{\max\left\{-1, \left(\frac{\tilde{d}^2_{\min} - d^2_{\max}}{4\sqrt{1-\delta}\sqrt{(\tilde{d}^2_{\min} + d^2_{\max})/2 - (1-\delta)}}\right)\right\}\right\}. \quad (3.6)$$

2) If $\tilde{d}^2_{\min} + d^2_{\max} > 4$, then

$$\alpha_{\max} = \cos^{-1}\left\{\max\left\{-1, \left(\frac{\tilde{d}^2_{\min} - d^2_{\max}}{4\sqrt{(\tilde{d}^2_{\min} + d^2_{\max})/2 - (1+\delta)}\sqrt{1+\delta}}\right)\right\}\right\}. \quad (3.7)$$

Proof: See Appendix E. □

IV. Derivation of $\alpha_{\min}$

By following the similar ideas and approaches as in Section III, we go on to derive $\alpha_{\min}$ in this section. According to Theorem 2.3 and (2.29), our task is to find the smallest $\measuredangle BDC$ among all $D \in \partial\mathbf{\Omega}^+_s(d_{\min})$, the top boundary of $\mathbf{\Omega}$. The main results of this section are summarized in Theorems 4.2 and 4.4.

Let us likewise decompose $\partial\mathbf{\Omega}^+_s(d_{\min})$ as the union of the three boundary curves $\mathcal{CV}(P, U_{l,s}(d_{\min}))$, $\mathcal{CV}(U_{l,s}(d_{\min}), U_{r,s}(d_{\min}))$ and $\mathcal{CV}(U_{r,s}(d_{\min}), Q)$ (see Fig. 5). To identify $\alpha_{\min}$, we shall first find the smallest $\measuredangle BDC$ for $D \in \mathcal{CV}(U_{l,s}(d_{\min}), U_{r,s}(d_{\min}))$ and further identify the minimal $\measuredangle BDC$ for $D \in \partial\mathbf{\Omega}^+_s(d_{\min}) = \mathcal{CV}(P, U_{l,s}(d_{\min})) \cup \mathcal{CV}(U_{l,s}(d_{\min}), U_{r,s}(d_{\min})) \cup \mathcal{CV}(U_{r,s}(d_{\min}), Q)$. Such an approach enjoys similar technical advantages as have been mentioned and evidenced in the previous section, wherein the closed-form formula of $\alpha_{\max}$ has been derived.

Note that $\mathcal{CV}(U_{l,s}(d_{\min}), U_{r,s}(d_{\min}))$ is the top edge of $\mathbf{\Omega}_s(d_{\min})$ (see Fig. 2(b) with $d = d_{\min}$). Hence, for any $D \in \mathcal{CV}(U_{l,s}(d_{\min}), U_{r,s}(d_{\min}))$, the quantity $|\overline{DB}|^2 + |\overline{DC}|^2$ must satisfy [cf., (2.21)]

$$|\overline{DB}|^2 + |\overline{DC}|^2 = \left(\frac{\tilde{d}^2_{\max} + d^2}{2} \cdot \frac{d^2_{\max}}{d^2} \right)_{d=d_{\min}} = \frac{\tilde{d}^2_{\max} + d^2_{\min}}{2} \cdot \xi^2 \tag{4.1}$$

where $\xi \overset{\triangle}{=} d_{\max}/d_{\min}$ is used throughout this section to conserve notation. With (4.1) and since $|\overline{BC}| = d_{\max}$, we have

$$\begin{aligned} \cos(\measuredangle BDC) &= \frac{|\overline{DB}|^2 + |\overline{DC}|^2 - |\overline{BC}|^2}{2|\overline{DB}| \times |\overline{DC}|} \\ &= \frac{(\tilde{d}^2_{\max} + d^2_{\min})/2 - d^2_{\min}}{2|\overline{DB}| \times |\overline{DC}|} \cdot \xi^2 \\ &= \frac{\tilde{d}^2_{\max} - d^2_{\min}}{4|\overline{DB}| \times |\overline{DC}|} \cdot \xi^2. \end{aligned} \tag{4.2}$$

Hence, for $D \in \mathcal{CV}(U_{l,s}(d_{\min}), U_{r,s}(d_{\min}))$, $\cos(\measuredangle BDC)$ depends on $(\tilde{d}^2_{\max} - d^2_{\min})\xi^2$ as well as the product length $|\overline{DB}| \cdot |\overline{DC}|$. Since ξ^2 (> 0) and $\tilde{d}^2_{\max} - d^2_{\min}$ are constants independent of D, to simplify the exposure, we proceed to find the minimal $\measuredangle BDC$, or the maximal $\cos(\measuredangle BDC)$, by first considering the scenario $\tilde{d}^2_{\max} - d^2_{\min} < 0$.

A. Case I: $\tilde{d}^2_{\max} - d^2_{\min} < 0$

As $\tilde{d}^2_{\max} - d^2_{\min} < 0$ and from (4.2), maximization of $\cos(\measuredangle BDC)$ thus amounts to maximizing the product length $|\overline{DB}| \cdot |\overline{DC}|$. Since

$$\begin{aligned} \left(|\overline{DB}| + |\overline{DC}|\right)^2 &= |\overline{DB}|^2 + |\overline{DC}|^2 + 2|\overline{DB}| \cdot |\overline{DC}| \\ &\overset{(a)}{=} \frac{\tilde{d}^2_{\max} + d^2_{\min}}{2} \cdot \xi^2 + 2|\overline{DB}| \cdot |\overline{DC}| \end{aligned} \tag{4.3}$$

where (a) follows from (4.1), maximization of $|\overline{DB}| \cdot |\overline{DC}|$ is equivalent to maximize the summed length $|\overline{DB}| + |\overline{DC}|$. Hence, maximization of $\cos\measuredangle(BDC)$ among all $D \in \mathcal{CV}(U_{l,s}(d_{\min}), U_{r,s}(d_{\min}))$ under the case $\tilde{d}^2_{\max} - d^2_{\min} < 0$ can be formulated as the following constrained optimization problem:

$$(P3)\ Maximize\ |\overline{DB}| + |\overline{DC}|,$$
$$subject\ to \begin{cases} (i)\ |\overline{DB}|^2 + |\overline{DC}|^2 = (\tilde{d}^2_{\max} + d^2_{\min}) \cdot \xi^2/2, \\ (ii)\ \sqrt{1-\delta} \cdot \xi \le |\overline{DB}| \le \sqrt{1+\delta} \cdot \xi, \\ (iii)\ \sqrt{1-\delta} \cdot \xi \le |\overline{DC}| \le \sqrt{1+\delta} \cdot \xi. \end{cases}$$

Note that the three constraints in $(P3)$ are the characterization of $|\overline{DB}|$ and $|\overline{DC}|$ for $D \in \mathcal{CV}(U_{l,s}(d_{\min}), U_{r,s}(d_{\min}))$ [cf., (2.21)]. The optimal D obtained by solving the above optimization problem is given in the next lemma.

Lemma 4.1: Let $d^2_{\min}$ and $\tilde{d}^2_{\max}$ be defined in, respectively, (2.5) and (2.8). If $\tilde{d}^2_{\max} - d^2_{\min} < 0$, and let $D_U \in \mathcal{CV}(U_{l,s}(d_{\min}), U_{r,s}(d_{\min}))$ be such that

$$|\overline{D_U B}| = |\overline{D_U C}| = \sqrt{(\tilde{d}^2_{\max} + d^2_{\min})/4} \cdot \xi \tag{4.4}$$

then the optimal $(|\overline{DB}|, |\overline{DC}|)$ which solves (P3) is uniquely given by $(|\overline{D_U B}|, |\overline{D_U C}|)$.

Proof: See Appendix F. □

Hence, we have $\measuredangle BD_U C < \measuredangle BDC$ for all $D \in \mathcal{CV}(U_{l,s}(d_{\min}), U_{r,s}(d_{\min}))\backslash\{D_U\}$. Through further analyses, it can be shown that $\measuredangle BD_U C$ is the global minimal angle $\alpha_{\min}$, as established in the next theorem.

Theorem 4.2: Let $d^2_{\min}$ and $\tilde{d}^2_{\max}$ be defined in, respectively, (2.5) and (2.8). If $\tilde{d}^2_{\max} - d^2_{\min} < 0$, we have

$$\alpha_{\min} = \measuredangle BD_U C = \cos^{-1}\left(\frac{\tilde{d}^2_{\max} - d^2_{\min}}{\tilde{d}^2_{\max} + d^2_{\min}} \right). \tag{4.5}$$

Proof: See Appendix G. □

B. Case II: $\tilde{d}^2_{\max} - d^2_{\min} \ge 0$

Since $\tilde{d}^2_{\max} - d^2_{\min} \ge 0$ and from (4.2) and (4.3), similar arguments show that minimization of $\measuredangle BDC$ for all $D \in \mathcal{CV}(U_{l,s}(d_{\min}), U_{r,s}(d_{\min}))$ can be formulated as the following constrained optimization problem:

$$(P4)\ Minimize\ |\overline{DB}| + |\overline{DC}|,$$
$$subject\ to \begin{cases} (i)\ |\overline{DB}|^2 + |\overline{DC}|^2 = (\tilde{d}^2_{\max} + d^2_{\min}) \cdot \xi^2/2, \\ (ii)\ \sqrt{1-\delta} \cdot \xi \le |\overline{DB}| \le \sqrt{1+\delta} \cdot \xi, \\ (iii)\ \sqrt{1-\delta} \cdot \xi \le |\overline{DC}| \le \sqrt{1+\delta} \cdot \xi. \end{cases}$$

The optimal D obtained by solving $(P4)$ is given in the next lemma.

Lemma 4.3: Let $d^2_{\min}$ and $\tilde{d}^2_{\max}$ be defined in, respectively, (2.5) and (2.8). If $\tilde{d}^2_{\max} - d^2_{\min} \ge 0$, the optimal $(|\overline{DB}|, |\overline{DC}|)$ which solves (P4) is given by $(|\overline{U_{l,s}(d_{\min})B}|, |\overline{U_{l,s}(d_{\min})C}|)$ or $(|\overline{U_{r,s}(d_{\min})B}|, |\overline{U_{r,s}(d_{\min})C}|)$.

Proof: See Appendix H. □

With the aid of Lemma 4.3, the minimal $\measuredangle BDC$ among all $D \in \mathcal{CV}(U_{l,s}(d_{\min}), U_{r,s}(d_{\min}))$ is attained by $D = U_{l,s}(d_{\min})$ or $D = U_{r,s}(d_{\min})$. By means of plane geometry analyses, $\alpha_{\min}$ in this case is derived in the following theorem.

Theorem 4.4: Let $d^2_{\min}$ and $\tilde{d}^2_{\max}$ be defined in, respectively, (2.5) and (2.8). If $\tilde{d}^2_{\max} - d^2_{\min} \ge 0$, the following results hold.

1) Case 1: $\tilde{d}^2_{\max} + d^2_{\min} < 4$

   We have

$$\alpha_{\min} = \cos^{-1}(\min\{1, \cos\alpha_1\}) \tag{4.6}$$

   where

$$\cos\alpha_1 = \frac{\tilde{d}^2_{\max} - d^2_{\min}}{4\sqrt{1-\delta}\sqrt{(\tilde{d}^2_{\max} + d^2_{\min})/2 - (1-\delta)}}. \tag{4.7}$$

2) Case 2: $\tilde{d}^2_{\max} + d^2_{\min} \geq 4$
   (a) If $(1+\delta) - d^2_{\min} \geq 0$, then

$$\alpha_{\min} = \cos^{-1}\left(\min\left\{1, \cos\alpha_2\right\}\right) \tag{4.8}$$

   where $\cos\alpha_2$ is given in (4.9), shown at the bottom of the page.
   (b) If $(1+\delta) - d^2_{\min} < 0$, then

$$\alpha_{\min} = \cos^{-1}\left(\min\left\{1, \cos\alpha_3\right\}\right) \tag{4.10}$$

   where

$$\cos\alpha_3 = \frac{\tilde{d}^2_{\max} - d^2_{\min}}{4\sqrt{1-\delta}\sqrt{(\tilde{d}^2_{\max} + d^2_{\min})/2 - (1-\delta)}}. \tag{4.11}$$

Proof: See Appendix I. □

V. Discussions

A. Connection to Previous Works

It is known that a sharp upper bound for $|\cos\alpha|$ ($\alpha = \measuredangle(\mathbf{\Phi u}, \mathbf{\Phi v})$) is crucial for accurate performance evaluations in many CS problems, e.g., [9], [21], [22], [25]. For the special case $\measuredangle(\mathbf{u}, \mathbf{v}) = \theta = \pi/2$, thus $\cos\theta = 0$, a well-known upper bound for $|\cos\alpha|$ derived by means of the polarization identity is given by [9]

$$|\cos\alpha| \leq \min\left\{\frac{\delta}{1-\delta}, 1\right\}. \tag{5.1}$$

Using the similar algebraic approach as in [9], a generalization of the above result to the case when θ is arbitrary (but fixed) is given in the following theorem.

Theorem 5.1: Assume that $\measuredangle(\mathbf{u}, \mathbf{v}) = \theta$. The following inequality holds:

$$|\cos\alpha| = \frac{|\langle \mathbf{\Phi u}, \mathbf{\Phi v}\rangle|}{\|\mathbf{\Phi u}\|_2 \|\mathbf{\Phi v}\|_2} \leq \min\left\{\frac{\delta + |\cos\theta|}{1-\delta}, 1\right\}. \tag{5.2}$$

Proof: See Appendix J. □

It is noted that, based also on the plane geometry setting introduced by Magen [34], [35] that is different from ours, bounds of the achievable angles between two compressed sparse vectors have been reported in [12] and [13]; the results are summarized in the next proposition.

Proposition 5.2 [13]: Assume that the sensing matrix $\mathbf{\Phi} \in \mathbb{R}^{m\times p}$ satisfies the RIP of order K with RIC $\delta \in [0, 1/3]$. Let $\mathbf{u} \in \mathbb{R}^p$ and $\mathbf{v} \in \mathbb{R}^p$ be two sparse vectors whose supports T_u and T_v satisfy $|T_u \cup T_v| \leq K$ and $\measuredangle(\mathbf{u}, \mathbf{v}) = \theta$ with $\theta \in [0, \pi/2]$. Then

$$(1 - \sqrt{3\delta})\theta \leq \measuredangle(\mathbf{\Phi u}, \mathbf{\Phi v}) \leq (1 + \sqrt{3\delta})\theta. \tag{5.3}$$

□

Now, with the aid of the derived $\alpha_{\max}$ and $\alpha_{\min}$ in the previous sections, the achievable $|\cos\alpha|$ can be directly determined as

$$\begin{cases} |\cos(\alpha_{\max})| \leq |\cos(\alpha)| \leq |\cos(\alpha_{\min})|, \\ \qquad\qquad \text{if } 0 < \alpha_{\min} < \alpha_{\max} \leq \pi/2, \\ |\cos(\alpha_{\min})| \leq |\cos(\alpha)| \leq |\cos(\alpha_{\max})|, \\ \qquad\qquad \text{if } \pi/2 \leq \alpha_{\min} < \alpha_{\max} < \pi, \\ 0 \leq |\cos(\alpha)| \leq \max\left\{|\cos(\alpha_{\min})|, |\cos(\alpha_{\max})|\right\}, \\ \qquad\qquad \text{if } 0 < \alpha_{\min} < \pi/2 < \alpha_{\max} < \pi. \end{cases} \tag{5.4}$$

For $\delta = 0.2, 0.3$, Fig. 6 compares the upper bounds in (5.2) and (5.3), and the proposed solution (5.4) for different θ. It can be seen that our solution (5.4) is tighter as compared with the other two bounds. The proposed bounds in (5.4) are further corroborated by computer simulations. To generate the test samples, the entries of the sensing matrix $\mathbf{\Phi} \in \mathbb{R}^{m\times p}$ are independently drawn from $\mathcal{N}(0, 1/m)$, namely, the Gaussian distribution with zero mean and variance equal to $1/m$. The ambient signal dimension is set to be $p = 2000$, and the sparsity level is $K = 10$. To guarantee that $\mathbf{\Phi}$ satisfies RIP with an RIC equal to δ (with a high probability), the required measurement size is set in accordance with $m \sim O(K\log(p/K)/\delta^2)$ [3]. Associated with each δ, a total number of 20000 K-sparse vector pairs $\{(\mathbf{u}_i, \mathbf{v}_i) | 1 \leq i \leq 20000\}$ are generated. For each test pair $(\mathbf{u}_i, \mathbf{v}_i)$, the angles $\theta_i = \measuredangle(\mathbf{u}_i, \mathbf{v}_i)$ and $\alpha_i = \measuredangle(\mathbf{\Phi u}_i, \mathbf{\Phi v}_i)$ are computed and then plotted on Fig. 6. As we can see, the proposed solutions (5.4) are indeed tight estimates of the achievable α_i's.

B. Special Case $\measuredangle(\mathbf{u}, \mathbf{v}) = \theta = \pi/2$

For the special case $\measuredangle(\mathbf{u}, \mathbf{v}) = \theta = \pi/2$, the closed-form formulae of $\alpha_{\max}$ and $\alpha_{\min}$ provided in Sections III and IV can be considerably simplified. Specifically, when $\theta = \pi/2$, it is easy to verify that

$$d^2_{\max} = \tilde{d}^2_{\max} = 2(1+\delta) \text{ and } d^2_{\min} = \tilde{d}^2_{\min} = 2(1-\delta). \tag{5.5}$$

Based on (5.5) together with some straightforward manipulations, we have the following corollary, which will be used to obtain improved performance guarantees in several CS systems in Section VI.

$$\cos\alpha_2 = \begin{cases} \max\left[\frac{\tilde{d}^2_{\max} - d^2_{\min}}{4\sqrt{1+\delta}\sqrt{(\tilde{d}^2_{\max} + d^2_{\min})/2 - (1+\delta)}}, \frac{\tilde{d}^2_{\min} - d^2_{\min}}{4\sqrt{1+\delta}\sqrt{(\tilde{d}^2_{\min} + d^2_{\min})/2 - (1+\delta)}}\right], & \text{if } \tilde{d}^2_{\min} + d^2_{\min} > 4 \\ \max\left\{\frac{\tilde{d}^2_{\max} - d^2_{\min}}{4\sqrt{1+\delta}\sqrt{(\tilde{d}^2_{\max} + d^2_{\min})/2 - (1+\delta)}}, \frac{2 - d^2_{\min}}{2\sqrt{1+\delta}\sqrt{1-\delta}}\right\}, & \text{if } \tilde{d}^2_{\min} + d^2_{\min} \leq 4 \end{cases} \tag{4.9}$$

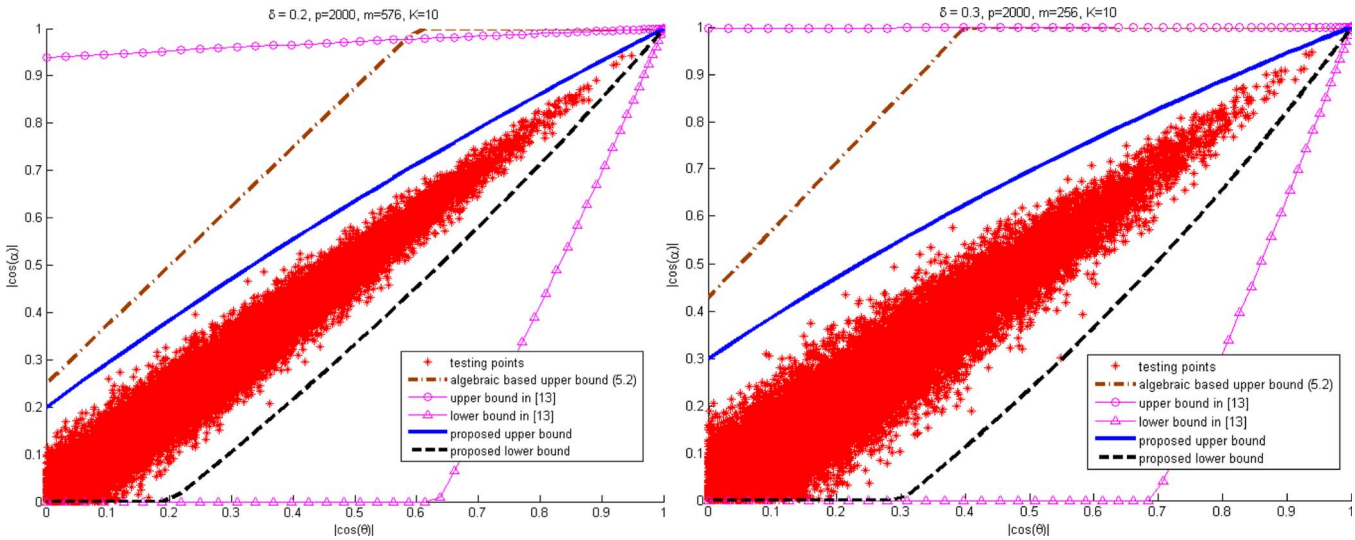

Fig. 6. Achievable $|\measuredangle \cos(\alpha)|$ obtained by the proposed solution (5.4), the upper bound (5.2) derived using the polarization identity, and the bounds (5.3) obtained by using the Magen's approach.

Corollary 5.3: For $\measuredangle(\mathbf{u},\mathbf{v}) = \pi/2$, $\alpha_{\max}$ and $\alpha_{\min}$ are, respectively, given as

$$\alpha_{\max} = \cos^{-1}\left(\max\left\{-1, \frac{-\delta}{\sqrt{1-\delta^2}}\right\}\right) \tag{5.6}$$

and

$$\alpha_{\min} = \cos^{-1}\left(\min\left\{1, \frac{\delta}{\sqrt{1-\delta^2}}\right\}\right). \tag{5.7}$$

□

VI. Applications

A. Improved RIC Estimate of Certain Structured Sensing Matrices

Consider the following CS system, in which the effective sensing matrix is the product of an orthogonal projection matrix $\mathbf{P}$ and the original sensing matrix $\mathbf{\Phi}$:

$$\mathbf{y} = \mathbf{P}\mathbf{\Phi}\mathbf{x} \tag{6.1}$$

where $\mathbf{P} \triangleq \mathbf{I} - \mathbf{\Phi}_{T_I}(\mathbf{\Phi}_{T_I}^*\mathbf{\Phi}_{T_I})^{-1}\mathbf{\Phi}_{T_I}^*$, with $\mathbf{I}$ being the identity matrix and $\mathbf{\Phi}_{T_I}$ consisting of the columns of $\mathbf{\Phi}$ indexed by a known set T_I. Note that the considered $\mathbf{P}$ acts as the orthogonal projection onto the orthogonal complement of the column space of $\mathbf{\Phi}_{T_I}$. The system model (6.1) arises, e.g., in compressed-domain interference cancellation [9]–[11], in modeling the residual vector of the OMP algorithm [21], and in establishing the democratic property of random sensing matrices [25], [26]. Characterization of the RIC of $\mathbf{P\Phi}$ is crucial for performance evaluation [9]–[11], [25], [26] and for the study of sufficient signal reconstruction conditions [21]. Based on the derived $\alpha_{\max}$ and $\alpha_{\min}$ in Sections III and IV, the RIC of $\mathbf{P\Phi}$ is specified in the following theorem.

Theorem 6.1: Consider the CS system (6.1). Assume that $\mathbf{\Phi}$ satisfies the RIP of order K with RIC given by δ. Let T_I be an index set with $|T_I| < K$, i.e., the cardinality of T_I is less than K. The following inequality holds for all $(K - |T_I|)$-sparse $\mathbf{x}$ whose support does not overlap with T_I:

$$(1-\overline{\delta})\,\|\mathbf{x}\|_2^2 \le \|\mathbf{P\Phi}\mathbf{x}\|_2^2 \le (1+\delta)\,\|\mathbf{x}\|_2^2 \tag{6.2}$$

where

$$\overline{\delta} = \min\left\{1, \delta + \frac{\delta^2}{1+\delta}\right\}. \tag{6.3}$$

Proof: See Appendix K. □

Theorem 6.1 asserts that $\mathbf{P\Phi}$ satisfies RIP with an RIC equal to $\overline{\delta}$ given in (6.3). Under the same assumptions as in Theorem 6.1 and by means of the polarization identity, an inequality analogous to (6.2) has been derived in [9] and [21] as:

$$\left(1 - \frac{\delta}{1-\delta}\right)\|\mathbf{x}\|_2^2 \le \|\mathbf{P\Phi}\mathbf{x}\|_2^2 \le (1+\delta)\,\|\mathbf{x}\|_2^2 \tag{6.4}$$

where $\mathbf{x}$ is $(K - |T_I|)$-sparse whose support does not overlap with T_I. Inequality (6.4) asserts that the RIC of $\mathbf{P\Phi}$ is equal to

$$\overline{\delta}_a = \min\left\{1, \frac{\delta}{1-\delta}\right\}. \tag{6.5}$$

Since

$$\frac{\delta}{1-\delta} = \delta + \frac{\delta^2}{1-\delta} \tag{6.6}$$

it is easy to see from (6.3) and (6.6) that $\overline{\delta} < \overline{\delta}_a$, that is, the proposed RIC $\overline{\delta}$ in (6.3) is tighter. The numerical values of the proposed solution (6.3) and the algebraic-based estimate $\overline{\delta}_a$ in (6.5) with respect to different δ are computed and plotted in Fig. 7. It is seen that considerable improvement can be achieved by our solution for moderate[7] δ.

B. Discussions

An immediate application of the above result, namely, the structured sensing matrix $\mathbf{P\Phi}$ can enjoy a smaller RIC, is in the problem of compressive-domain interference cancellation

[7] A large δ will result in the failure of signal recovery and thus should be precluded [24].

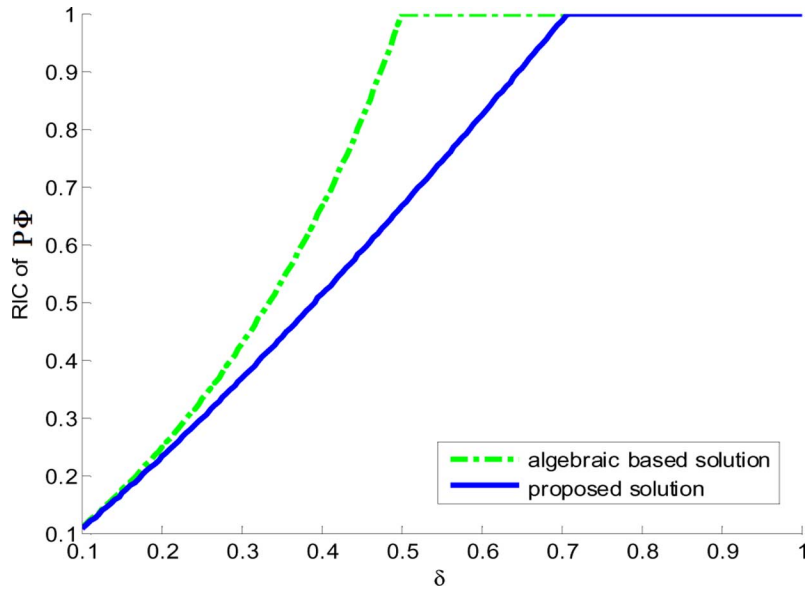

Fig. 7. Comparison of the RIC of the effective sensing matrix $\mathbf{P\Phi}$.

[9]–[11], wherein $\mathbf{P\Phi}$ is the sensing matrix of the effective data acquisition system after the undesirable interference is removed via orthogonal projection. The related details are referred to [33].

As another application, let us recall that the RIC of $\mathbf{P\Phi}$ is also needed in establishing the *democratic property* of random sensing matrices [25], [26], an appealing characteristic which guarantees the robustness of random data acquisition against the loss of measurements. Let $\tilde{\mathbf{\Phi}} \in \mathbb{R}^{M\times N}$, with entries drawn from $\mathcal{N}(0, 1/M)$, satisfy RIP of order K with RIC given by δ. By democracy it is meant that, as long as M is large enough, a submatrix obtained by deleting a small, and randomly chosen, subset of rows of $\tilde{\mathbf{\Phi}}$ still satisfies RIP but with a larger RIC. More precisely, assume that 1) $\tilde{M}$ is a positive integer such that $\tilde{M} \leq M$, $K \leq \tilde{M}$, and $D = M - \tilde{M} \geq 0$, and 2) $M = C_1(K + D)\log((N + M)/(K + D))$ for some constant C_1. Then, with a high probability, a submatrix $\tilde{\mathbf{\Phi}}_{\tilde{M}} \in \mathbb{R}^{\tilde{M}\times N}$ obtained by removing arbitrary D rows of $\tilde{\mathbf{\Phi}}$ satisfies RIP of order K with RIC equal to $\delta/(1-\delta)$ [25]. By following the same proof procedures as in [25], it can be directly verified that the RIC of $\tilde{\mathbf{\Phi}}_{\tilde{M}}$ can be further tightened to $\overline{\delta}$ given in (6.3) [recall from Fig. 7 that $\overline{\delta}$ is uniformly smaller than $\delta/(1-\delta)$]. Note that $\tilde{\mathbf{\Phi}}_{\tilde{M}}$ represents the sensing matrix of the effective sensing system when D measurements are dropped [25]. The established result, namely, $\tilde{\mathbf{\Phi}}_{\tilde{M}}$ enjoys a smaller RIC, confirms that better robustness of random sensing against measurement loss can be achieved.

VII. Conclusion

In this paper, the achievable angles between two compressed sparse vectors under RIP-induced norm/distance constraints are analytically characterized in a plane geometry framework. Motivated by the law of cosines and geometric interpretations of RIP, it is shown that all the algebraic constraints imposed by RIP that are pertinent to the identification of the achievable angles can be depicted in the 2-D plane. By exploiting the conformal property of similarity, it allows us to construct a single geometric diagram, based on which a unified joint analysis of all the considered algebraic constraints can be conducted from a geometric point of view. By means of the proposed approach, the maximal and minimal achievable angles can be derived in closed form and are then corroborated by numerical simulations. Compared with the existing algebraic-based method employing the polarization identity, the proposed approach does provide sharper estimates of the achievable angles. Applications of our study to CS are investigated. First of all, we derive a closed-form RIC of the product of an orthogonal projection matrix and a random sensing matrix. Our solution is shown to be tighter than an RIC estimate reported in the literature. An immediate application of the result above is in compressed-domain interference cancellation; details can be referred to [33]. As another application, we show that, with a small randomly chosen subset of rows removed from a random sensing matrix, the resultant submatrix enjoys an RIC smaller than the one reported in the literature. The result asserts that random sensing can provide better robustness against the measurement loss. It is believed that the presented analytic study of the achievable angles between two compressed sparse vectors can be of fundamental importance in the study of many other CS problems; this is currently under investigation.

Appendix
Supporting Technical Proofs

The following two lemmas will be used throughout the Appendix.

Lemma A.1: Consider the two triangles ΔKJL and ΔKSL in Fig. 8, in which ΔKSL lies entirely inside ΔKJL. Then, $\measuredangle KSL > \measuredangle KJL$.

Proof: The result follows since

$$\begin{aligned}\measuredangle KSL &= \pi - (\measuredangle SKL + \measuredangle SLK)\\ &= \pi - (\pi - \measuredangle JKS - \measuredangle JLS - \measuredangle KJL)\\ &= \measuredangle JKS + \measuredangle JLS + \measuredangle KJL > \measuredangle KJL.\end{aligned}$$

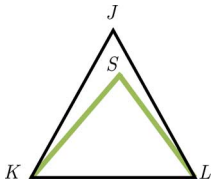

Fig. 8. Depiction of two triangles considered in Lemma A.1.

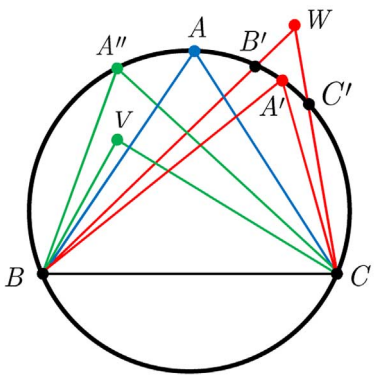

Fig. 9. Depiction of geometric objects considered in Lemma A.2.

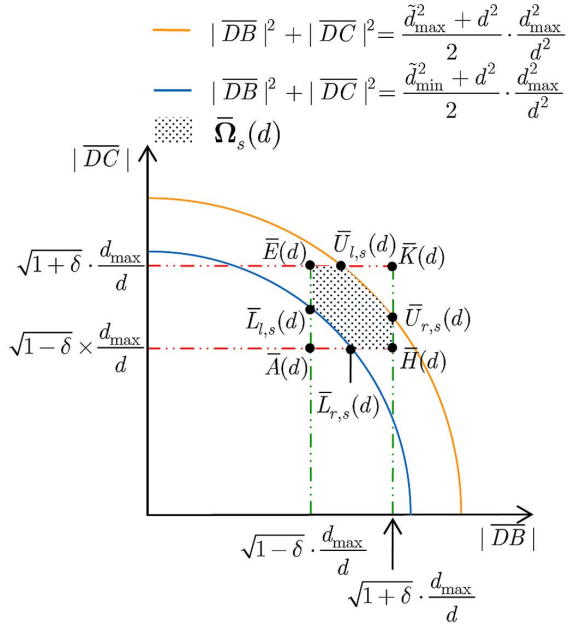

Fig. 10. Alternative depiction of the similar feasible top-vex set $\mathbf{\Omega}_s(d)$ via the considered coordinate system.

□

Lemma A.2: Let $\overline{BC}$ be a chord of a circle. Pick V and W as two points above $\overline{BC}$, with V inside the circle and W outside the circle as depicted in Fig. 9. Also, let A be an arbitrary point on the arc of the circle above $\overline{BC}$. Then, $\measuredangle BWC < \measuredangle BAC < \measuredangle BVC$.

Proof: The triangle ΔWBC intersects with the circle, say, at B' and C'. Let A' be a point on arc $B'C'$. By lemma A.1, we have

$$\measuredangle BWC < \measuredangle BA'C. \tag{A.1}$$

Let us further pick A'' as a point on the circle such that ΔBVC lies entirely inside $\Delta BA''C$. Again by Lemma A.1, we have

$$\measuredangle BA''C < \measuredangle BVC. \tag{A.2}$$

A well-known result from plane geometry is that angles inscribed by the same arc of a circle are equal [20]; thus

$$\measuredangle BA'C = \measuredangle BAC = \measuredangle BA''C. \tag{A.3}$$

The assertion follows from (A.1)–(A.3). □

Throughout the Appendix, knowledge of the dilated length $|\overline{DB}|$ and $|\overline{DC}|$ for $D \in \mathbf{\Omega}_s(d)$ is needed. Toward this end, we will leverage an alternative schematic description of the similar feasible top-vertex set $\mathbf{\Omega}_s(d)$ to ease analysis. To construct this diagram, for $D \in \mathbf{\Omega}_s(d)$, we shall first specify the constraints on $|\overline{DB}|$ and $|\overline{DC}|$ under RIP. Pick a plausible $\|\mathbf{\Phi}(\mathbf{u}-\mathbf{v})\|_2 = d$. Recall that, for each $D \in \mathbf{\Omega}_s(d)$ in Fig. 2(b), there is one and only one corresponding feasible top vertex $D_d \in \mathbf{\Omega}(d)$ in Fig. 2(a). Since Fig. 2(b) is obtained as the dilation of Fig. 2(a) with the scale $d_{\max}/d$, we have $|\overline{DB}| = |\overline{D_dB_d}| \cdot (d_{\max}/d)$ and $|\overline{DC}| = |\overline{D_dC_d}| \cdot (d_{\max}/d)$. Hence, for $D \in \mathbf{\Omega}_s(d)$ the norm constraints on $|\overline{DB}|$ and $|\overline{DC}|$ can be directly modified based on (2.2) as (note in our setting $|\overline{D_dB_d}| = \|\mathbf{\Phi}\mathbf{u}\|_2$ and $|\overline{D_dC_d}| = \|\mathbf{\Phi}\mathbf{v}\|_2$)

$$\begin{aligned}\sqrt{1-\delta}\cdot\frac{d_{\max}}{d} \le |\overline{DB}| \le \sqrt{1+\delta}\cdot\frac{d_{\max}}{d}\\ \sqrt{1-\delta}\cdot\frac{d_{\max}}{d} \le |\overline{DC}| \le \sqrt{1+\delta}\cdot\frac{d_{\max}}{d}.\end{aligned} \tag{A.4}$$

Similarly, the constraint on $|\overline{DB}|^2 + |\overline{DC}|^2$ can be obtained from (2.13) as

$$\frac{\tilde{d}^2_{\min}+d^2}{2}\cdot\frac{d^2_{\max}}{d^2} \le |\overline{DB}|^2+|\overline{DC}|^2 \le \frac{\tilde{d}^2_{\max}+d^2}{2}\cdot\frac{d^2_{\max}}{d^2}. \tag{A.5}$$

Now, we consider the first quadrant of the coordinate system in the plane, with $|\overline{DB}|$ as the abscissa and $|\overline{DC}|$ as the ordinate. Taking into account (A.4) and (A.5), the depiction of all $D \in \mathbf{\Omega}_s(d)$ alternatively on this coordinate system is thus shown as the shadowed region $\bar{\mathbf{\Omega}}_s(d)$ in Fig. 10, in which $\overline{U}_{l,s}(d)$, $\overline{U}_{r,s}(d)$, $\overline{L}_{l,s}(d)$, and $\overline{L}_{r,s}(d)$ correspond to, respectively, the four points $U_{l,s}(d)$, $U_{r,s}(d)$, $L_{l,s}(d)$, and $L_{r,s}(d)$ on $\mathbf{\Omega}_s(d)$. The main advantage of the alternative depiction $\bar{\mathbf{\Omega}}_s(d)$ in Fig. 10 is that it allows for a simple way of specifying $|\overline{DB}|$ and $|\overline{DC}|$ associated with all $D \in \mathbf{\Omega}_s(d)$. This will in turn simplify the underlying analyses, as will be seen later.

A) Proof of Theorem 2.3: The proof of Theorem 2.3 basically consists of the following two parts.

1) First, we will prove that all elements on the left boundary $\partial\mathbf{\Omega}_l$ and the right boundary $\partial\mathbf{\Omega}_r$, except the end points (P, Q, F, G), can be excluded from the candidate set in regard to the identification of $\alpha_{\max}$ and $\alpha_{\min}$.
2) Then, we will show that $\alpha_{\max}$ and $\alpha_{\min}$ will never be attained by the points in the interior of $\mathbf{\Omega}$. In particular, $\alpha_{\max}$ and $\alpha_{\min}$ will be attained by some D located on, respectively, the bottom and top boundaries of $\mathbf{\Omega}$. This thus completes the proof.

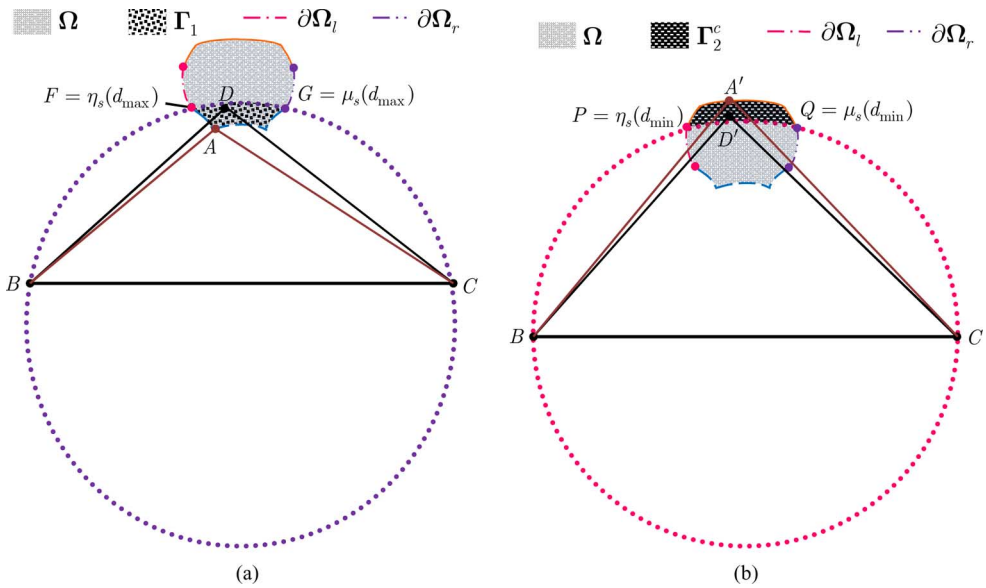

Fig. 11. Depiction of all geometric objects for plane geometric analyses conducted in the proof Theorem 2.3.

The first part is established directly by the following lemma, whose proof is placed at the end of Appendix A so as to ease readability.

Lemma A.3: The following results hold:

1) $\measuredangle BPC < \measuredangle BDC < \measuredangle BFC$ for all $D \in \partial\mathbf{\Omega}_l \setminus \{P, F\}$.
2) $\measuredangle BQC < \measuredangle BDC < \measuredangle BGC$ for all $D \in \partial\mathbf{\Omega}_r \setminus \{Q, G\}$.

□

To prove the second part, we shall first show that $\alpha_{\max}$ is attained by some point on the bottom boundary $\partial\mathbf{\Omega}_b$. For this let us construct a circle $\mathcal{C}_1$ (marked in purple) with $\overline{BC}$ as a chord and with F and G on arc BC as depicted in Fig. 11(a); also, let

$$\mathbf{\Gamma}_1 \stackrel{\triangle}{=} \{D \in \mathbf{\Omega} \mid D \text{ lies on or inside } \mathcal{C}_1\}, \tag{A.6}$$

and denote by $\mathbf{\Gamma}_1^c$ the complement of $\mathbf{\Gamma}_1$ in $\mathbf{\Omega}$. By Lemma A.2, it follows immediately that $\measuredangle BDC < \measuredangle BGC$ for all $D \in \mathbf{\Gamma}_1^c$. Notably, all the points on the left and right boundaries, i.e., $\partial\mathbf{\Omega}_l$ and $\partial\mathbf{\Omega}_r$, except F and G, must belong to $\mathbf{\Gamma}_1^c$; this is because if there exists some $D' \in \partial\mathbf{\Omega}_r \setminus \{G\}$ inside $\mathbf{\Gamma}_1$, then again by Lemma A.2 we must have $\measuredangle BD'C \geq \measuredangle BGC$, which contradicts with part (2) of Lemma A.3. As a result, we can rule out those $D \in \mathbf{\Gamma}_1^c$, which includes $\partial\mathbf{\Omega}_l \backslash \{F\}$ and $\partial\mathbf{\Omega}_r \backslash \{G\}$, regarding the search of $\alpha_{\max}$. It then remains to consider $\mathbf{\Gamma}_1$. Observe that, for any $D \in \mathbf{\Gamma}_1$, both the two sides $\overline{DB}$ and $\overline{DC}$ of ΔDBC intersect with $\partial\mathbf{\Omega}_b$, meaning that there exists an $A \in \partial\mathbf{\Omega}_b$ such that ΔABC lies entirely inside ΔDBC [see also Fig. 11(a)]. By Lemma A.1, we have $\measuredangle BAC > \measuredangle BDC$. This shows that $\alpha_{\max}$ must be attained by some point on $\partial\mathbf{\Omega}_b$.

Now let us go on to show that $\alpha_{\min}$ is achieved by some point $D \in \partial\mathbf{\Omega}_t$. The idea is quite similar to that in the previous proof. First, we construct circles $\mathcal{C}_2$ with $\overline{BC}$ as a chord and with P and Q on arc BC [see Fig. 11(b)]. Similar to (A.6), we define

$$\mathbf{\Gamma}_2 \stackrel{\triangle}{=} \{D \in \mathbf{\Omega} \mid D \text{ lies on or inside } \mathcal{C}_2\}. \tag{A.7}$$

Also, we denote by $\mathbf{\Gamma}_2^c$ the complement of $\mathbf{\Gamma}_2$ in $\mathbf{\Omega}$. From Lemma A.2, we immediately have $\measuredangle BD'C > \measuredangle BPC$ for all $D' \in \mathbf{\Gamma}_2$. In addition, from Lemma A.2 and Lemma A.3, $\partial\mathbf{\Omega}_l \backslash \{P\}$ and $\partial\mathbf{\Omega}_r \backslash \{Q\}$ both must belong to $\mathbf{\Gamma}_2$. Hence, it only remains to consider $\mathbf{\Gamma}_2^c$ regarding the identification of $\alpha_{\min}$. Observe that, for any $D' \in \mathbf{\Gamma}_2^c$, there exists at least one element A' on $\partial\mathbf{\Omega}_t$ such that $\Delta D'BC$ is completely inside $\Delta A'BC$ [see also Fig. 11(b)]. From Lemma A.1, we must have $\measuredangle BA'C < \measuredangle BD'C$. This established that $\alpha_{\min} = \measuredangle BA'C$ for some point $A' \in \partial\mathbf{\Omega}_t$. □

Now, let us provide the proof of Lemma A.3. Owing to the symmetric nature of $\mathbf{\Omega}$, it suffices to prove the first assertion. Since $F = \eta_s(d_{\max})$, $P = \eta_s(d_{\min})$, and $\partial\mathbf{\Omega}_l$ consists of all $\eta_s(d)$'s, $d_{\min} \leq d \leq d_{\max}$, the left corner points of $\mathbf{\Omega}_s(d)$'s [see (2.31)], it remains to show that, as d increases from $d_{\min}$ to $d_{\max}$, $\measuredangle B\eta_s(d)C$ is monotonically increasing (or equivalently, $\cos(\measuredangle B\eta_s(d)C)$ is monotonically decreasing). Toward this end, we shall first find an explicit expression for $\cos(\measuredangle B\eta_s(d)C)$ as a function of d. From the law of cosines

$$\cos(\measuredangle B\eta_s(d)C) = \frac{|\overline{\eta_s(d)B}|^2 + |\overline{\eta_s(d)C}|^2 - |\overline{BC}|^2}{2|\overline{\eta_s(d)B}| \cdot |\overline{\eta_s(d)C}|}$$

and recall that $|\overline{BC}|$ is set to be $|\overline{BC}| = d_{\max}$, we observe that only $|\overline{\eta_s(d)B}|$ and $|\overline{\eta_s(d)C}|$ are needed to determine $\cos(\measuredangle B\eta_s(d)C)$. To ease the derivation, we will resort to the diagram $\overline{\mathbf{\Omega}}_s(d)$ in Fig. 10 to specify $|\overline{\eta_s(d)B}|$ and $|\overline{\eta_s(d)C}|$. This can be done if we can first identify the corresponding location of $\eta_s(d)$ on $\overline{\mathbf{\Omega}}_s(d)$ as d varies; the results are established in the next lemma.

Lemma A.4: Let $\eta_s(d)$ be defined in (2.27), and $\overline{\eta}_s(d)$ be the corresponding location on $\overline{\mathbf{\Omega}}_s(d)$. Also, let $\overline{U}_{l,s}(d)$ and $\overline{L}_{l,s}(d)$ be the points on $\overline{\mathbf{\Omega}}_s(d)$ that correspond to, respectively, $U_{l,s}(d)$ and $L_{l,s}(d)$ on $\mathbf{\Omega}_s(d)$ [see (2.21) and (2.22), and Fig. 2(b)]. Denote by $\overline{E}(d)$ the point

$(\sqrt{1-\delta}\cdot\frac{d_{\max}}{d},\sqrt{1+\delta}\cdot\frac{d_{\max}}{d})$ on the coordinate system on Fig. 10. The following results hold:

$$\bar{\eta}_s(d)=\begin{cases}\bar{U}_{l,s}(d), & \text{if } (\tilde{d}^2_{\max}+d^2)/2<(1-\delta)+(1+\delta)\\ \bar{E}(d), & \text{if } \frac{\tilde{d}^2_{\min}+d^2}{2}\le(1-\delta)+(1+\delta)\le\frac{\tilde{d}^2_{\max}+d^2}{2}\\ \bar{L}_{l,s}(d), & \text{if } (\tilde{d}^2_{\min}+d^2)/2>(1-\delta)+(1+\delta).\end{cases} \tag{A.8}$$

Proof of Lemma A.4: We first note that

$$\begin{aligned}|\overline{BD}|\cos(\measuredangle DBC)&=|\overline{BD}|\cdot\frac{d^2_{\max}+|\overline{BD}|^2-|\overline{DC}|^2}{2|\overline{BD}|\cdot d_{\max}}\\&=\frac{d^2_{\max}+|\overline{BD}|^2-|\overline{DC}|^2}{2\cdot d_{\max}}\end{aligned} \tag{A.9}$$

which implies that $|\overline{BD}|\cos(\measuredangle DBC)$ attains the minimum if $|\overline{BD}|^2-|\overline{DC}|^2$ is minimized. Hence, $\eta_s(d)$ in (2.27) can be equivalently rewritten as $\eta_s(d)=\arg\min_{D\in\mathbf{\Omega}_s(d)}\{|\overline{BD}|^2-|\overline{DC}|^2\}$, and thus

$$\bar{\eta}_s(d)=\arg\min_{D\in\bar{\mathbf{\Omega}}_s(d)}\{|\overline{BD}|^2-|\overline{DC}|^2\}. \tag{A.10}$$

To minimize $|\overline{BD}|^2-|\overline{DC}|^2$, $|\overline{BD}|^2$ should be as small as possible, whereas $|\overline{DC}|^2$ should be instead as large as possible. It can be seen from Fig. 10 that the point $\overline{E}(d)$ is associated with the smallest $|\overline{BD}|^2$ and the largest $|\overline{DC}|^2$. Hence, conceptually, among all points on $\overline{\mathbf{\Omega}}_s(d)$, the one located closest to $\overline{E}(d)$ will yield minimal $|\overline{BD}|^2-|\overline{DC}|^2$, and therefore according to (A.10) should be identified as $\overline{\eta}_s(d)$. Since $\overline{E}(d)$ is not always feasible (i.e., $\overline{E}(d)$ may lie outside $\overline{\mathbf{\Omega}}_s(d)$), $\overline{\eta}_s(d)$ depends on the location of $\overline{E}(d)$ relative to $\overline{\mathbf{\Omega}}_s(d)$. Under the assumption $(\tilde{d}^2_{\max}+d^2)/2<(1-\delta)+(1+\delta)$, $\overline{E}(d)$ locates above $\overline{\mathbf{\Omega}}_s(d)$ [see Fig. 12(a)], and the desired solution is thus $\overline{U}_{l,s}(d)$. In case that $(\tilde{d}^2_{\min}+d^2)/2\le(1-\delta)+(1+\delta)\le(\tilde{d}^2_{\max}+d^2)/2$, $\overline{E}(d)$ is feasible [see Fig. 12(b)] and thus $\overline{\eta}(d)=\overline{E}(d)$. If $(\tilde{d}^2_{\min}+d^2)/2>(1-\delta)+(1+\delta)$, $\overline{E}(d)$ locates on the left of $\overline{\mathbf{\Omega}}_s(d)$ [see Fig. 12(c)], and the desired solution is $\overline{\eta}_s(d)=\overline{L}_{l,s}(d)$. □

Proof of Lemma A.3: To prove (1), it suffices to show that, as d increases from $d_{\min}$ to $d_{\max}$, the resultant $\cos\alpha$ is monotonically decreasing. Now, if d is small such that $(\tilde{d}^2_{\max}+d^2)/2<(1-\delta)+(1+\delta)$, Lemma A.4 asserts that $\overline{\eta}_s(d)=\overline{U}_{l,s}(d)$ [cf., Fig. 12(a)]; since the magnitude triple $(|\eta_s(d)B|,|\eta_s(d)C|,|\overline{BC}|)$ associated with $\overline{\eta}_s(d)=\overline{U}_{l,s}(d)$ is given by $(\sqrt{1-\delta}\cdot\frac{d_{\max}}{d},\sqrt{(\tilde{d}^2_{\max}+d^2)/2-(1-\delta)}\cdot\frac{d_{\max}}{d},d\cdot\frac{d_{\max}}{d})$, the resultant α is easily determined by the law of cosines to be

$$\cos\alpha=\frac{\tilde{d}^2_{\max}-d^2}{4\sqrt{(\tilde{d}^2_{\max}+d^2)/2-(1-\delta)}\sqrt{1-\delta}}. \tag{A.11}$$

As d increases such that $(\tilde{d}^2_{\min}+d^2)/2\le(1-\delta)+(1+\delta)\le(\tilde{d}^2_{\max}+d^2)/2$, we have from Lemma A.4 that $\overline{\eta}_s(d)=\overline{E}(d)$ [see Fig. 12(b)]; the associated magnitude triple is $(|\overline{\eta_s(d)B}|,|\overline{\eta_s(d)C}|,|\overline{BC}|)=(\sqrt{1-\delta}\cdot\frac{d_{\max}}{d},\sqrt{1+\delta}\cdot\frac{d_{\max}}{d},d\cdot\frac{d_{\max}}{d})$, yielding

$$\cos\alpha=\frac{(1+\delta)+(1-\delta)-d^2}{2\sqrt{1+\delta}\sqrt{1-\delta}}. \tag{A.12}$$

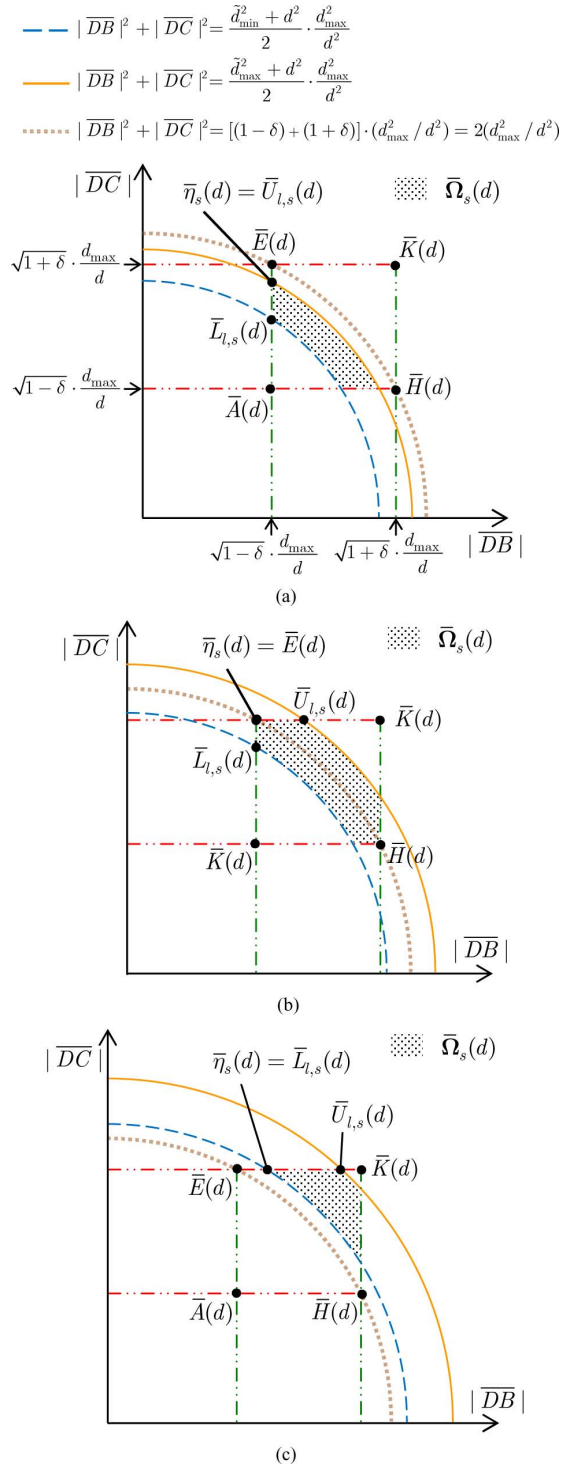

Fig. 12. Depiction of $\overline{\mathbf{\Omega}}_s(d)$ with respective to three cases: (a) $(\tilde{d}^2_{\max}+d^2)/2<(1-\delta)+(1+\delta)$, (b) $(\tilde{d}^2_{\min}+d^2)/2\le(1-\delta)+(1+\delta)\le(\tilde{d}^2_{\max}+d^2)/2$, (c) $(\tilde{d}^2_{\min}+d^2)/2>(1-\delta)+(1+\delta)$.

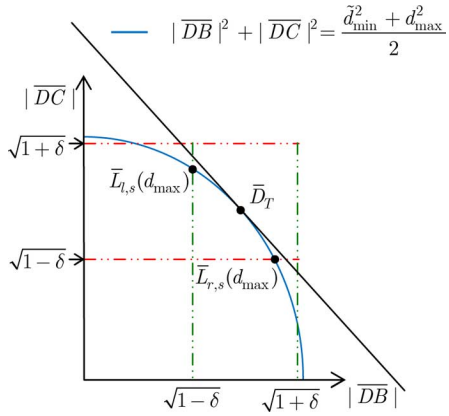

Fig. 13. Location of the tangency point $\overline{D}_T$ with respect to the curve $\mathcal{CV}(\bar{L}_l(d_{\max}), \bar{L}_r(d_{\max}))$.

As d further increases such that $(\tilde{d}^2_{\min}+d^2)/2 > (1-\delta)+(1+\delta)$, then from lemma A.4, we have $\overline{\eta}_s(d)=\overline{L}_{l,s}(d)$ [see Fig. 12(c)]. Thus, $(|\overline{\eta_s(d)B}|, |\overline{\eta_s(d)C}|, |\overline{BC}|) = (\sqrt{(\tilde{d}^2_{\min}+d^2)/2-(1+\delta)}\cdot\frac{d_{\max}}{d}, \sqrt{1+\delta}\cdot\frac{d_{\max}}{d}, d\cdot\frac{d_{\max}}{d})$, which results in

$$\cos\alpha=\frac{\tilde{d}^2_{\min}-d^2}{4\sqrt{(\tilde{d}^2_{\min}+d^2)/2-(1+\delta)}\sqrt{1+\delta}}. \quad \text{(A.13)}$$

From (A.11)–(A.13), it can be seen that $\cos\alpha$ is monotonically decreasing with d (this can be readily checked by computing the first-order derivatives). This thus proves Lemma A.3. □

B) Proof of Lemma 3.1: Since the feasible set for Problem (P1) consists of merely these $D \in \mathcal{CV}(L_{l,s}(d_{\max}), L_{r,s}(d_{\max}))$, let us focus on the corresponding curve $\mathcal{CV}(\bar{L}_{l,s}(d_{\max}), \bar{L}_{r,s}(d_{\max})) \subset \bar{\boldsymbol{\Omega}}_s(d_{\max})$, which lies on the quarter-circle with radius $\sqrt{(\tilde{d}^2_{\min}+d^2_{\max})/2}$ as depicted in Fig. 13. It is clear that the maximal $|\overline{DB}|+|\overline{DC}|$ on the quarter-circle is attained by the unique tangency point, say, $\overline{D}_T$, of the tangent line $|\overline{DB}|+|\overline{DC}| = \sqrt{\tilde{d}^2_{\min}+d^2_{\max}}$. Note that the coordinate of $\overline{D}_T$ is $(|\overline{DB}|, |\overline{DC}|) = (\sqrt{\frac{\tilde{d}^2_{\min}+d^2_{\max}}{4}}, \sqrt{\frac{\tilde{d}^2_{\min}+d^2_{\max}}{4}})$, and thus, $\overline{D}_T$ exactly corresponds to D_L defined in (3.4). As a result, the point D_L will yield the maximal $\measuredangle BDC$. The proof is thus completed. □

C) Proof of Theorem 3.2: First of all, we have from Lemma 3.1 that

$$\measuredangle BD_LC > \measuredangle BDC \text{ for all } D \in \mathcal{CV}(L_{l,s}(d_{\max}), L_{r,s}(d_{\max}))\backslash\{D_L\}. \quad \text{(A.14)}$$

Let us then construct a circle $\mathcal{C}_{D_L}$, marked in dashed blue in Fig. 14, with $\overline{BC}$ as a chord and D_L on arc BC. From (A.14) and Lemma A.2, we must have $\mathcal{C}_{D_L} \cap \mathcal{CV}(L_{l,s}(d_{\max}), L_{r,s}(d_{\max})) = \{D_L\}$, and, in particular, $L_{l,s}(d_{\max})$ and $L_{r,s}(d_{\max})$ must locate outside $\mathcal{C}_{D_L}$. We claim

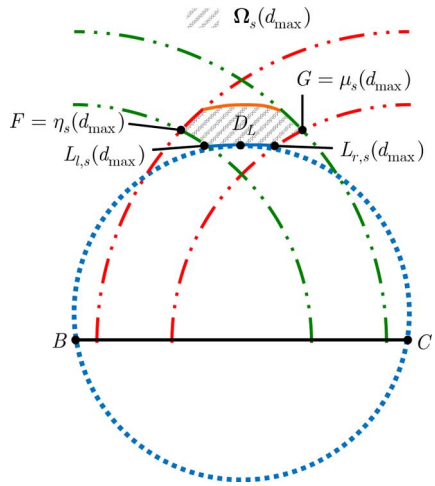

Fig. 14. Depiction of all geometric objects for plane geometric analyses conducted in the proof Theorem 3.2.

that both $\mathcal{CV}(F, L_{l,s}(d_{\max}))$ and $\mathcal{CV}(L_{r,s}(d_{\max}), G)$ are also outside $\mathcal{C}_{D_L}$. As a result, it follows again from Lemma A.2 that

$$\measuredangle BD_LC > \measuredangle BDC \text{ for all } D \in \mathcal{CV}(F, L_{l,s}(d_{\max})) \cup \mathcal{CV}(L_{r,s}(d_{\max}), G). \quad \text{(A.15)}$$

Based on (A.14) and (A.15), it can be deduced that $\alpha_{\max} = \measuredangle BD_LC$. Since $(|\overline{BD_L}|, |\overline{D_LC}|, |\overline{BC}|) = (\sqrt{(\tilde{d}^2_{\min}+d^2_{\max})/4}, \sqrt{(\tilde{d}^2_{\min}+d^2_{\max})/4}, d_{\max})$, equation (3.5) follows. To prove the claim, due to the symmetric nature of the figure it suffices to show $\mathcal{CV}(F, L_{l,s}(d_{\max}))$ is outside $\mathcal{C}_{D_L}$. For this, we need the next lemma.

Lemma A.5: If $\mathcal{CV}(F, L_{l,s}(d_{\max}))$ contains more than one element, then for all $D \in \mathcal{CV}(F, L_{l,s}(d_{\max}))$, we have $|\overline{DB}| = \sqrt{1-\delta}$.

Proof: The assertion of the lemma can be obtained by resorting to $\overline{\boldsymbol{\Omega}}_s(d_{\max})$ shown in Fig. 12. To prove the lemma, let us first identify the curve in $\overline{\boldsymbol{\Omega}}_s(d_{\max})$ that corresponds to $\mathcal{CV}(F, L_{l,s}(d_{\max}))$. Denote by $\overline{F} \in \overline{\boldsymbol{\Omega}}_s(d_{\max})$ the point corresponding to $F \in \boldsymbol{\Omega}_s(d_{\max})$. By definition, $F = \eta_s(d_{\max})$ and, thus, $\overline{F} = \overline{\eta}_s(d_{\max})$. According to Lemma A.4, and with $d = d_{\max}$, we then have (A.16), which further implies (A.17) [(A.16) and (A.17) are shown at the bottom of the next page].

Under the condition that $\mathcal{CV}(F, L_{l,s}(d_{\max}))$ contains more than one element and from (A.17), the curve on $\overline{\boldsymbol{\Omega}}_s(d_{\max})$ corresponding to $\mathcal{CV}(F, L_{l,s}(d_{\max}))$ is either $\mathcal{CV}(\overline{U}_{l,s}(d_{\max}), \overline{L}_{l,s}(d_{\max}))$ or $\mathcal{CV}(\overline{E}(d_{\max}), \overline{L}_{l,s}(d_{\max}))$ [this is depicted, respectively, in Fig. 12(a) and (b)]. We can observe from the figures that $\mathcal{CV}(\bar{U}_{l,s}(d_{\max}), \bar{L}_{l,s}(d_{\max}))$ and $\mathcal{CV}(\bar{E}(d_{\max}), \bar{L}_{l,s}(d_{\max}))$ both locate on the line segment $\overline{\bar{A}(d_{\max})\bar{E}(d_{\max})}$. The assertion follows since all points on $\bar{A}(d_{\max})\bar{E}(d_{\max})$ are associated with $|\overline{DB}| = \sqrt{1-\delta}$. □

Proof of Claim: If $\mathcal{CV}(F, L_{l,s}(d_{\max}))$ degenerates into one point $\{L_{l,s}(d_{\max})\}$, we are done since $L_{l,s}(d_{\max})$ is outside $\mathcal{C}_{D_L}$. For the general case, it readily follows from Lemma A.5 that $\mathcal{CV}(F, L_{l,s}(d_{\max}))$ lies on the arc of the circle $\mathcal{C}(B, \sqrt{1-\delta})$. Since $L_{l,s}(d_{\max})$ is outside $\mathcal{C}_{D_L}$ and,

moreover, $F = \eta_s(d_{\max})$ locates to the left of $L_{l,s}(d_{\max})$ (see Fig. 14), $\mathcal{CV}(F, L_{l,s}(d_{\max})) \subset \mathcal{C}(B, \sqrt{1-\delta})$ must lie entirely outside $\mathcal{C}_{D_L}$. □

D) Proof of Lemma 3.3: Now the problem is to minimize $|\overline{DB}| + |\overline{DC}|$ under the same constraints as in problem (P1). The solution can be found by again resorting to Fig. 13 used in the proof of Lemma 3.1 (see Appendix B). It is easy to see from the figure that, to minimize $|\overline{DB}| + |\overline{DC}|$ among all $D \in \mathcal{CV}(\bar{L}_{l,s}(d_{\max}), \bar{L}_{r,s}(d_{\max}))$, we shall choose the one that is located as far away from the tangency point $\bar{D}_T$ as possible. The solution is either one of the two end points of $\mathcal{CV}(\bar{L}_{l,s}(d_{\max}), \bar{L}_{r,s}(d_{\max}))$, namely, $\bar{L}_{l,s}(d_{\max})$ or $\bar{L}_{r,s}(d_{\max})$. The corresponding point on $\mathbf{\Omega}_s(d_{\max})$ is $D = L_{l,s}(d_{\max})$ or $D = L_{r,s}(d_{\max})$. The assertion thus follows. □

E) Proof of Theorem 3.4: Now if we construct a circle C_3 with $\overline{BC}$ as a chord and with $L_{l,s}(d_{\max})$ and $L_{r,s}(d_{\max})$ on arc BC as in Fig. 15, by following similar procedures as in the proof of Theorem 3.2, it can be verified that $\mathcal{CV}(L_{l,s}(d_{\max}), L_{r,s}(d_{\max}))\backslash\{L_{l,s}(d_{\max}), L_{r,s}(d_{\max})\}$, $\mathcal{CV}(F, L_{l,s}(d_{\max}))$, and $\mathcal{CV}(L_{r,s}(d_{\max}), G)$ all lie outside this circle. That is, the whole region $\mathbf{\Omega}_s(d_{\max})$, except $L_{l,s}(d_{\max})$ and $L_{r,s}(d_{\max})$, falls outside circle C_3. Again from Lemma A.2, we thus have

$$\begin{aligned}\alpha_{\max} &= \measuredangle B L_{r,s}(d_{\max}) C \\ &= \measuredangle B L_{l,s}(d_{\max}) C \\ &= \cos^{-1}\left(\frac{|\overline{L_{l,s}(d_{\max})B}|^2 + |\overline{L_{l,s}(d_{\max})C}|^2 - d_{\max}^2}{2|\overline{L_{l,s}(d_{\max})B}| \cdot |\overline{L_{l,s}(d_{\max})C}|}\right).\end{aligned} \tag{A.18}$$

To specify $|\overline{L_{l,s}(d_{\max})B}|$ and $|\overline{L_{l,s}(d_{\max})C}|$, we can first refer to $\bar{\mathbf{\Omega}}_s(d_{\max})$ in Fig. 12 to determine the location of $\bar{L}_{l,s}(d_{\max})$ which corresponds to $L_{l,s}(d_{\max})$; this in turn allows us to determine $|\overline{L_{l,s}(d_{\max})B}|$ and $|\overline{L_{l,s}(d_{\max})C}|$. Under the assumption $(\tilde{d}_{\min}^2 + d_{\max}^2)/2 \le (1-\delta)+(1+\delta)$, i.e., $(\tilde{d}_{\min}^2 + d_{\max}^2) \le 4$, we have $|\overline{L_{l,s}(d_{\max})B}| = \sqrt{1-\delta}$ [see Fig. 12(a) and (b)], and by computation $|\overline{L_{l,s}(d_{\max})C}| = \sqrt{(\tilde{d}_{\min}^2 + d_{\max}^2)/2 - (1-\delta)}$ (since $|\overline{L_{l,s}(d_{\max})B}|^2 + |\overline{L_{l,s}(d_{\max})C}|^2 = (\tilde{d}_{\min}^2 + d_{\max}^2)/2$), which together with (A.18) leads to (3.6). In case that $(\tilde{d}_{\min}^2 + d_{\max}^2)/2 > (1-\delta)+(1+\delta)$, i.e., $(\tilde{d}_{\min}^2 + d_{\max}^2) > 4$, we have $|\overline{L_{l,s}(d_{\max})C}| = \sqrt{1+\delta}$, and $|\overline{L_{l,s}(d_{\max})B}| = \sqrt{(\tilde{d}_{\min}^2 + d_{\max}^2)/2 - (1+\delta)}$ (since $|\overline{L_{l,s}(d_{\max})B}|^2 + |\overline{L_{l,s}(d_{\max})C}|^2 = (\tilde{d}_{\min}^2 + d_{\max}^2)/2$), which combined with (A.18) yields (3.7). We note that, since $\tilde{d}_{\min}^2 - d_{\max}^2 < 0$ and from (3.2), we must have

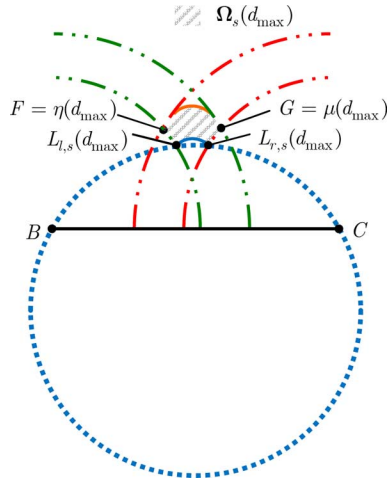

Fig. 15. Depiction of all geometric objects for plane geometric analyses conducted in the proof Theorem 3.4.

$\cos(\measuredangle B L_{l,s}(d_{\max}) C) < 0$ in the considered scenario. In case that

$$\frac{|\overline{L_{l,s}(d_{\max})B}|^2 + |\overline{L_{l,s}(d_{\max})C}|^2 - d_{\max}^2}{2|\overline{L_{l,s}(d_{\max})B}| \cdot |\overline{L_{l,s}(d_{\max})C}|} < -1 \tag{A.19}$$

we must have $\cos\alpha_{\max} = -1$, and hence $\alpha_{\max} = \pi$. □

F) Proof of Lemma 4.1: The idea behind this proof is essentially the same as that in the proof of Lemma 3.1. The details are thus omitted to conserve space.

G) Proof of Theorem 4.2: The idea behind the proof is quite similar to that in the proof of Theorem 3.2. From Lemma 4.1, it follows immediately

$$\begin{aligned}&\measuredangle B D_U C < \measuredangle B D C \text{ for all} \\ &\quad D \in \mathcal{CV}(U_{l,s}(d_{\min}), U_{r,s}(d_{\min}))\backslash\{D_U\}.\end{aligned} \tag{A.20}$$

Construct a circle $\mathcal{C}_{D_U}$ with $\overline{BC}$ as a chord and with D_U on arc BC (see Fig. 16). Then, from (A.20) and Lemma A.2, $\mathcal{CV}(U_{l,s}(d_{\min}), U_{r,s}(d_{\min}))\backslash\{D_U\}$ must lie entirely within $\mathcal{C}_{D_U}$; if there exists some $D' \in \mathcal{CV}(U_{l,s}(d_{\min}), U_{r,s}(d_{\min}))\backslash\{D_U\}$ on or outside $\mathcal{C}_{D_U}$, then Lemma A.2 implies $\measuredangle B D_U C \ge \measuredangle B D' C$, which contradicts with (A.20). We further claim that both $\mathcal{CV}(P, U_{l,s}(d_{\min}))$ and $\mathcal{CV}(U_{r,s}(d_{\min}), Q)$ are also inside $\mathcal{C}_{D_U}$. Hence, again by Lemma A.2, we have

$$\begin{aligned}&\measuredangle B D_U C < \measuredangle B D C \text{ for all} \\ &\quad D \in \mathcal{CV}(P, U_{l,s}(d_{\min})) \cup \mathcal{CV}(U_{r,s}(d_{\min}), Q).\end{aligned} \tag{A.21}$$

$$\bar{F} = \bar{\eta}_s(d_{\max}) = \begin{cases} \bar{U}_{l,s}(d_{\max}), & \text{if } (\tilde{d}_{\max}^2 + d_{\max}^2)/2 < (1-\delta)+(1+\delta) \\ \bar{E}(d_{\max}), & \text{if } (\tilde{d}_{\min}^2 + d_{\max}^2)/2 \le (1-\delta)+(1+\delta) \le (\tilde{d}_{\max}^2 + d_{\max}^2)/2 \\ \bar{L}_{l,s}(d_{\max}), & \text{if } (\tilde{d}_{\min}^2 + d_{\max}^2)/2 > (1-\delta)+(1+\delta). \end{cases} \tag{A.16}$$

$$\mathcal{CV}(\bar{F}, \bar{L}_{l,s}(d_{\max})) = \begin{cases} \mathcal{CV}(\bar{U}_{l,s}(d_{\max}), \bar{L}_{l,s}(d_{\max})), & \text{if } (\tilde{d}_{\max}^2 + d_{\max}^2)/2 < (1-\delta)+(1+\delta) \\ \mathcal{CV}(\bar{E}(d_{\max}), \bar{L}_{l,s}(d_{\max})), & \text{if } (\tilde{d}_{\min}^2 + d_{\max}^2)/2 \le (1-\delta)+(1+\delta) \le (\tilde{d}_{\max}^2 + d_{\max}^2)/2 \\ \bar{L}_{l,s}(d_{\max}), & \text{if } (\tilde{d}_{\min}^2 + d_{\max}^2)/2 > (1-\delta)+(1+\delta) \end{cases} \tag{A.17}$$

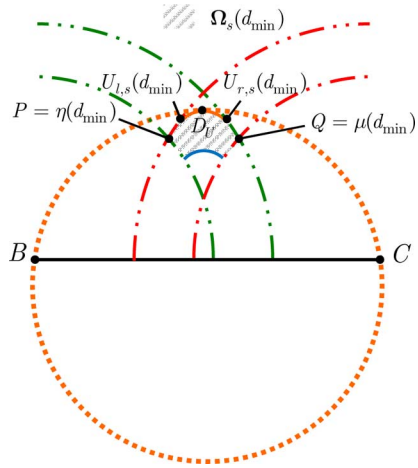

Fig. 16. Depiction of all geometric objects for plane geometric analyses conducted in the proof Theorem 4.2.

Based on (A.20) and (A.21), it can be deduced that $\alpha_{\min} = \measuredangle BD_UC$. To prove the claim, due to the symmetric nature of the figure, it suffices to show that $\mathcal{CV}(P, U_{l,s}(d_{\min}))$ is inside $\mathcal{C}_{D_U}$. This can be done with the aid of the next lemma.

Lemma A.6: If $\mathcal{CV}(P, U_{l,s}(d_{\min}))$ contains more than one element, then for all $D \in \mathcal{CV}(P, U_{l,s}(d_{\min}))$, we have $|\overline{DC}| = \sqrt{1+\delta}\cdot\xi$.

Proof: The assertion of the lemma can be obtained by resorting to $\bar{\mathbf{\Omega}}_s(d_{\min})$ shown in Fig. 12. The details are essentially the same as those in the proof of Lemma A.5, and are thus omitted to conserve space. □

Proof of Claim: If $\mathcal{CV}(P, U_{l,s}(d_{\min}))$ degenerates into one point $\{U_l\}$, we are done since $U_{l,s}(d_{\min})$ is inside $\mathcal{C}_{D_U}$. For the general case, it readily follows from Lemma A.6 that $\mathcal{CV}(P, U_{l,s}(d_{\min}))$ lies on the arc of the circle $\mathcal{C}(C, \sqrt{1+\delta}\cdot\xi)$. Since $U_{l,s}(d_{\min})$ is inside $\mathcal{C}_{D_U}$, and, moreover, $P = \eta_s(d_{\min})$ locates to the left of $U_{l,s}(d_{\min})$ (see Fig. 16), $\mathcal{CV}(P, U_{l,s}(d_{\min})) \subset \mathcal{C}(C, \sqrt{1+\delta}\cdot\xi)$ must lie entirely inside $\mathcal{C}_{D_U}$. □

H) Proof of Lemma 4.3: The proof can be done based on Lemma 4.1, and by following the arguments as in the proof of Lemma 3.3. □

I) Proof of Theorem 4.4: From Lemma 4.3, we have

$$\measuredangle BDC > \measuredangle BU_{l,s}(d_{\min})C = \measuredangle BU_{r,s}(d_{\min})C \text{ for all } D \in \mathcal{CV}(U_{l,s}(d_{\min}), U_{r,s}(d_{\min}))\backslash\{U_{l,s}(d_{\min}), U_{r,s}(d_{\min})\}. \tag{A.22}$$

It then suffices to consider $\mathcal{CV}(P, U_{l,s}(d_{\min}))$ for identifying $\alpha_{\min}$ since the region $\mathbf{\Omega}$ is symmetric. If $\mathcal{CV}(P, U_{l,s}(d_{\min}))$ degenerates into one single element $\{U_{l,s}(d_{\min})\}$, or equivalently, $P = \eta_s(d_{\max}) = U_{l,s}(d_{\min})$ (by Lemma A.4 and see Fig. 12, this case occurs when $(\tilde{d}^2_{\max} + d^2_{\min})/2 < (1+\delta)+(1-\delta)$, i.e., $\tilde{d}^2_{\max} + d^2_{\min} < 4$), $\measuredangle BU_{l,s}(d_{\min})C$ is then the desired solution; the magnitude triple associated with $U_{l,s}(d_{\min})$ is $(|\overline{BU_{l,s}(d_{\min})}|, |\overline{CU_{l,s}(d_{\min})}|, |\overline{BC}|) = (\sqrt{1-\delta}\cdot\xi, \sqrt{(\tilde{d}^2_{\max}+d^2_{\min})/2-(1-\delta)}\cdot\xi, d_{\min}\cdot\xi)$, thus resulting in

$$\cos\alpha_{\min} = \frac{(\tilde{d}^2_{\max} - d^2_{\min})}{4\sqrt{1-\delta}\sqrt{(\tilde{d}^2_{\max}+d^2_{\min})/2-(1-\delta)}} \tag{A.23}$$

which yields (4.6). Let us turn to consider the general case when $\mathcal{CV}(P, U_{l,s}(d_{\min}))$ contains more than one element, or equivalently, $P = \eta_s(d_{\min}) \neq U_{l,s}(d_{\min})$ (according to Lemma A.4, this occurs when $(\tilde{d}^2_{\max} + d^2_{\min})/2 \geq (1+\delta)+(1-\delta)$, i.e., $(\tilde{d}^2_{\max} + d^2_{\min}) \geq 4$). From Lemma A.6, it follows that $|\overline{DC}| = \sqrt{1+\delta}\cdot\xi$ for all $D \in \mathcal{CV}(P, U_{l,s}(d_{\min}))$. Since $|\overline{BC}| = d_{\max} = d_{\min}\cdot\xi$, the cosine of $\measuredangle BDC$ for $D \in \mathcal{CV}(P, U_{l,s}(d_{\min}))$ reads

$$\begin{aligned}\cos(\measuredangle BDC) &= \frac{|\overline{DB}|^2 + |\overline{DC}|^2 - |\overline{BC}|^2}{2|\overline{DB}|\cdot|\overline{DC}|} \\ &= \frac{|\overline{DB}|^2 + (1+\delta)\cdot\xi^2 - d^2_{\min}\cdot\xi^2}{|\overline{DB}|}\cdot\gamma_2 \\ &\text{where } \gamma_2 \triangleq \frac{1}{2\sqrt{1+\delta}\xi} > 0.\end{aligned} \tag{A.24}$$

Equation (A.24) shows that, for $D \in \mathcal{CV}(P, U_{l,s}(d_{\min}))$, the resultant $\cos(\measuredangle BDC)$ is completely determined by $|\overline{DB}|$. Hence, to find the minimal $\measuredangle BDC$, it is equivalent to find the optimal $|\overline{DB}|$ which maximizes $\cos(\measuredangle BDC)$. By treating $|\overline{DB}|$ as a dummy variable, let us first compute the first- and second-order derivatives of $\cos(\measuredangle BDC)$ with respect to $|\overline{DB}|$ as

$$(\cos(\measuredangle BDC))' = \left(1 - \frac{(1+\delta)\cdot\xi^2 - d^2_{\min}\cdot\xi^2}{|\overline{DB}|^2}\right)\cdot\gamma_2 \tag{A.25}$$

and

$$(\cos(\measuredangle BDC))'' = 2((1+\delta) - d^2_{\min})\cdot\xi^2\cdot\gamma_2/|\overline{DB}|^3. \tag{A.26}$$

Let us first consider the case $(1+\delta) - d^2_{\min} \geq 0$, which together with (A.26) asserts that $\cos(\measuredangle BDC)$ is a convex function of $|\overline{DB}|$. The convexity of $\cos(\measuredangle BDC)$ implies that the maximal $\cos(\measuredangle BDC)$ (or, minimal achievable $\measuredangle BDC$) is attained by either the minimal $|\overline{DB}|$ or the maximal $|\overline{DB}|$ among all $D \in \mathcal{CV}(P, U_{l,s}(d_{\min}))$. Let us refer to Fig. 12(b) and (c) with $d = d_{\min}$, and focus on the corresponding curve $\mathcal{CV}(\bar{P}, \bar{U}_{l,s}(d_{\min}))$ (recall that $P = \eta_s(d_{\min})$). It is easy to see that the minimal and maximal $|\overline{DB}|$ are attained by, respectively, $\bar{P}$ and $\bar{U}_{l,s}(d_{\min})$. This thus implies that the minimal and maximal $|\overline{DB}|$ among all $D \in \mathcal{CV}(P, U_{l,s}(d_{\min}))$ are attained by either one of the two end points, namely $D = P$ and $D = U_{l,s}(d_{\min})$; as a result, we have

$$\cos\alpha_{\min} = \max\{\cos\measuredangle BPC, \cos\measuredangle BU_{l,s}(d_{\min})C\}. \tag{A.27}$$

To compute $\alpha_{\min}$ based on (A.27), we shall first find explicit expressions for $\cos\measuredangle BPC$ and $\cos\measuredangle BU_{l,s}(d_{\min})C$. Since in the case $(\tilde{d}^2_{\max} + d^2_{\min})/2 \geq (1+\delta)+(1-\delta)$, we can refer to Fig. 12(b) and (c) to determine the magnitude triple associated with $U_{l,s}(d_{\min})$ as $(|\overline{U_{l,s}(d_{\min})B}|, |\overline{U_{l,s}(d_{\min})C}|, |\overline{BC}|) = (\sqrt{(\tilde{d}^2_{\max}+d^2_{\min})/2-(1+\delta)}\cdot\xi, \sqrt{1+\delta}\cdot\xi, d_{\min}\cdot\xi)$; by the law of cosines it follows

$$\cos(\measuredangle BU_{l,s}(d_{\min})C) = \frac{(\tilde{d}^2_{\max} - d^2_{\min})}{4\sqrt{1+\delta}\sqrt{(\tilde{d}^2_{\max}+d^2_{\min})/2-(1+\delta)}}. \tag{A.28}$$

To find $\measuredangle BPC$, we first note that the location corresponding to P on the diagram $\bar{\mathbf{\Omega}}_s(d_{\min})$ is $\bar{\eta}(d_{\min})$. From Lemma A.4, the exact location of $\bar{\eta}(d_{\min})$ depends on the value of $d_{\min}$. If $(\tilde{d}^2_{\min}+d^2_{\min})/2 > (1+\delta)+(1-\delta)$, then $\bar{\eta}(d_{\min}) = \bar{L}_{l,s}(d_{\min})$, and thus, $P = L_{l,s}(d_{\min})$. The associated magnitude triple is $(|\overline{PB}|, |\overline{PC}|, |\overline{BC}|) = (\sqrt{\frac{\tilde{d}^2_{\min}+d^2_{\min}}{2}} - (1+\delta)\cdot\xi, \sqrt{1+\delta}\cdot\xi, d_{\min}\cdot\xi)$, which implies

$$\begin{aligned}\cos(\measuredangle BPC) &= \cos(\measuredangle BL_{l,s}(d_{\min})C) \\ &= \frac{(\tilde{d}^2_{\min} - d^2_{\min})}{4\sqrt{1+\delta}\sqrt{(\tilde{d}^2_{\min}+d^2_{\min})/2-(1+\delta)}}.\end{aligned} \tag{A.29}$$

If $(\tilde{d}^2_{\min}+d^2_{\min})/2 \le (1+\delta)+(1-\delta)$ $(\le (\tilde{d}^2_{\max}+d^2_{\min})/2)$, we have from Lemma A.4 that $\bar{\eta}_s(d_{\min}) = \bar{E}(d_{\min})$. The associated magnitude triple is $(|\overline{PB}|, |\overline{PC}|, |\overline{BC}|) = (\sqrt{1-\delta}\cdot\xi, \sqrt{1+\delta}\cdot\xi, d_{\min}\cdot\xi)$; by using the law of cosines, we have

$$\cos(\measuredangle BPC) = \frac{(1+\delta)+(1-\delta)-d^2_{\min}}{2\sqrt{1+\delta}\sqrt{1-\delta}}. \tag{A.30}$$

Let us turn to consider the other case $(1+\delta)-d^2_{\min} < 0$. As such, we have $(\cos(\measuredangle BDC))' > 0$ [see (A.25)], and $\cos(\measuredangle BDC)$ is, therefore, an increasing function of $|\overline{DB}|$. Since $|\overline{DB}| \le |\overline{U_{l,s}(d_{\min})B}|$ for all $D \in \mathcal{CV}(P, U_{l,s}(d_{\min}))$ [again, this can be easily verified based on Fig. 12(b) and (c)], the optimal solution is $U_{l,s}(d_{\min})$, and the resultant $\measuredangle BU_{l,s}(d_{\min})C$ is given precisely as in (A.28).

Finally, we note that under the considered assumption $\tilde{d}^2_{\max} - d^2_{\min} \ge 0$, we have from (4.2) that $\cos(\measuredangle BDC) \ge 0$ for all $D \in \mathcal{CV}(U_{l,s}(d_{\min}), U_{r,s}(d_{\min}))$. In case that the values of computed $\cos\alpha_{\min}$ are greater than 1, we must have $\cos\alpha_{\min} = 1$, and hence $\alpha_{\min} = 0$. □

J) Proof of Theorem 5.1: Since $\|\mathbf{u}\pm\mathbf{v}\|_2^2 = \|\mathbf{u}\|_2^2 + \|\mathbf{v}\|_2^2 \pm 2\|\mathbf{u}\|_2\|\mathbf{v}\|_2\cos\theta = 2\pm 2\cos\theta$ under the assumption that $\|\mathbf{u}\|_2^2 = 1$ and $\|\mathbf{v}\|_2^2 = 1$,we have

$$2 - 2|\cos\theta| \le \|\mathbf{u}\pm\mathbf{v}\|_2^2 \le 2 + 2|\cos\theta|. \tag{A.31}$$

Based on (A.31) and RIP, it follows that

$$\begin{aligned}(1-\delta)\{2-2|\cos\theta|\} &\le \|\mathbf{\Phi}(\mathbf{u}\pm\mathbf{v})\|_2^2 \\ &\le (1+\delta)\{2+2|\cos\theta|\}.\end{aligned} \tag{A.32}$$

Now

$$\begin{aligned}|\langle\mathbf{\Phi u}, \mathbf{\Phi v}\rangle| &\overset{(a)}{=} \frac{1}{4}\left\{\|\mathbf{\Phi u}+\mathbf{\Phi v}\|_2^2 - \|\mathbf{\Phi u}-\mathbf{\Phi v}\|_2^2\right\} \\ &\overset{(b)}{\le} \frac{1}{4}\{(1+\delta)[2+2|\cos\theta|]-(1-\delta)[2-2|\cos\theta|]\} \\ &= \{\delta + |\cos\theta|\}\end{aligned} \tag{A.33}$$

where (a) follows from the polarization identity, and (b) holds from (A.32). Since

$$\|\mathbf{\Phi u}\|_2\|\mathbf{\Phi v}\|_2 \ge (1-\delta)\|\mathbf{u}\|_2\|\mathbf{v}\|_2 = 1-\delta \tag{A.34}$$

inequality (5.2) follows from (A.33) and (A.34), and since $|\cos\alpha| \le 1$. □

K) Proof of Theorem 6.1: The proof can be done by leveraging the geometric property of the orthogonal projection. Specifically, let us decompose $\mathbf{\Phi x}$ into

$$\mathbf{\Phi x} = \mathbf{P\Phi x} + (\mathbf{I}-\mathbf{P})\mathbf{\Phi x}. \tag{A.35}$$

By definition $\mathbf{P} \overset{\triangle}{=} \mathbf{I} - \mathbf{\Phi}_{T_I}(\mathbf{\Phi}^*_{T_I}\mathbf{\Phi}_{T_I})^{-1}\mathbf{\Phi}^*_{T_I}$, we immediately have

$$\mathbf{I}-\mathbf{P} = \mathbf{\Phi}_{T_I}(\mathbf{\Phi}^*_{T_I}\mathbf{\Phi}_{T_I})^{-1}\mathbf{\Phi}^*_{T_I} \tag{A.36}$$

which is the orthogonal projection onto $\mathcal{R}(\mathbf{\Phi}_{T_I})$, namely, the column space of $\mathbf{\Phi}_{T_I}$. As a result, the term $(\mathbf{I}-\mathbf{P})\mathbf{\Phi x}$ can be expressed as

$$(\mathbf{I}-\mathbf{P})\mathbf{\Phi x} = \mathbf{\Phi}_{T_I}\tilde{\mathbf{x}}'_I = \mathbf{\Phi x}'_I \tag{A.37}$$

where $\tilde{\mathbf{x}}'_I \in \mathbb{R}^{|T_I|}$, and $\mathbf{x}'_I \in \mathbb{R}^p$ is $|T_I|$-sparse (with support T_I) that is obtained by padding $p-|T_I|$ zeros to $\tilde{\mathbf{x}}'_I$. Since $\mathbf{P}$ is an orthogonal projection matrix, it follows that (see Fig. 17)

$$\begin{aligned}\|\mathbf{P\Phi x}\|_2^2 &= \|\mathbf{\Phi x}\|_2^2|\sin\measuredangle(\mathbf{\Phi x}, \mathbf{\Phi x}'_I)|^2 \\ &= \|\mathbf{\Phi x}\|_2^2(1-|\cos\measuredangle(\mathbf{\Phi x}, \mathbf{\Phi x}'_I)|^2).\end{aligned} \tag{A.38}$$

Since by assumption $\mathbf{x}$ is a $(K-|T_I|)$-sparse vector, with the aid of (1.2) and (A.38) we then have (A.39), and therefore (A.40) holds. From (5.4), we have (A.41) [see the bottom of the page for (A.39), (A.40), and (A.41)].

To explicitly specify $\max|\cos\measuredangle(\mathbf{\Phi x}', \mathbf{\Phi x})|^2$, we first note from the assumption that the supports of $\mathbf{x}$ and $\mathbf{x}'_I$ do not

---

$$(1-|\cos\measuredangle(\mathbf{\Phi x}, \mathbf{\Phi x}'_I)|^2)(1-\delta)\|\mathbf{x}\|_2^2 \le \|\mathbf{P\Phi x}\|_2^2 \le (1-|\cos\measuredangle(\mathbf{\Phi x}, \mathbf{\Phi x}'_I)|^2)(1+\delta)\|\mathbf{x}\|_2^2 \tag{A.39}$$

$$\left(1-\max|\cos\measuredangle(\mathbf{\Phi x}', \mathbf{\Phi x})|^2\right)(1-\delta)\|\mathbf{x}\|_2^2 \le \|\mathbf{P\Phi x}\|_2^2 \le (1+\delta)\|\mathbf{x}\|_2^2 \tag{A.40}$$

$$\max|\cos\measuredangle(\mathbf{\Phi x}', \mathbf{\Phi x})|^2 = \begin{cases} |\cos(\alpha_{\min})|^2, & \text{if } 0 < \alpha_{\min} < \alpha_{\max} \le \pi/2 \\ |\cos(\alpha_{\max})|^2, & \text{if } \pi/2 < \alpha_{\min} < \alpha_{\max} < \pi \\ \max\left\{|\cos(\alpha_{\min})|^2, |\cos(\alpha_{\max})|^2\right\}, & \text{if } 0 < \alpha_{\min} < \pi/2 < \alpha_{\max} < \pi \end{cases} \tag{A.41}$$

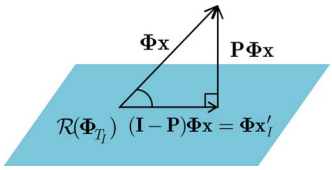

Fig. 17. Schematic description of orthogonal projection of $\mathbf{\Phi x}$ onto the column space of $\mathbf{\Phi}_{I_I}$.

overlap, which implies $\measuredangle(\mathbf{x}, \mathbf{x}'_I) = \pi/2$. Hence, according to (A.41) and Corollary 5.3, it follows

$$\max |\cos \measuredangle(\mathbf{\Phi x}', \mathbf{\Phi x})|^2 = \min \left\{ 1, \frac{\delta^2}{1-\delta^2} \right\}. \qquad \text{(A.42)}$$

Combining (A.40) and (A.42) yields (6.3). □

ACKNOWLEDGMENT

The second author would like to thank Prof. Po-Ning Chen for his constructive suggestions during the revision of this paper. Also, he would like to dedicate this paper to Prof. Ching-An Lin, for his patience, kindness, and support during the past two decades.

REFERENCES

[1] R. G. Baraniuk, "Compressive sensing," *IEEE Signal Process. Mag.*, vol. 24, no. 4, pp. 118–124, Jul. 2007.
[2] E. J. Candes and M. B. Wakin, "An introduction to compressive sampling," *IEEE Signal Process. Mag.*, vol. 25, no. 2, pp. 21–30, Mar. 2008.
[3] M. Davenport, M. Duarte, Y. C. Eldar, and G. Kutyniok, "Introduction to compressed sensing," in *Compressed Sensing: Theory and Applications*. Cambridge, U.K.: Cambridge Univ. Press, 2011.
[4] J. A. Tropp, J. N. Laska, M. F. Duarte, J. K. Romberg, and R. G. Baraniuk, "Beyond Nyquist: Efficient sampling of spare bandlimited signals," *IEEE Trans. Inf. Theory*, vol. 56, no. 1, pp. 520–544, Jan. 2010.
[5] M. Elad, M. A. T. Figueiredo, and Y. Ma, "On the role of sparse and redundant representations in image processing," *Proc. IEEE*, vol. 98, no. 6, pp. 972–982, Jun. 2010.
[6] W. U. Bajwa, J. Haupt, A. M. Sayeed, and R. Nowak, "Compressed channel sensing: A new approach to estimating sparse multipath channels," *Proc. IEEE*, vol. 98, no. 6, pp. 1058–1076, Jun. 2010.
[7] J. Haupt, W. U. Bajwa, G. Raz, and R. Nowak, "Toeplitz compressed sensing matrices with applications to sparse channel estimation," *IEEE Trans. Inf. Theory*, vol. 56, no. 11, pp. 5862–5875, Nov. 2010.
[8] M. Sharp and A. Scaglione, "Application of sparse signal recovery to pilot-assisted channel estimation," in *Proc. Int. Conf. Acoust., Speech, Signal Process.*, 2008, pp. 3469–3472.
[9] M. A. Davenport, P. T. Boufounos, and R. G. Baraniuk, "Compressive domain interference cancellation," presented at the Workshop Signal Process. Adapt. Sparse Struct. Represent., Saint-Malo, France, 2009.
[10] M. A. Davenport, S. R. Schnelle, J. R. Slavinsky, R. G. Baraniuk, M. B. Wakin, and P. T. Boufounous, "A wideband compressive radio receiver," in *Proc. IEEE Mil. Commun. Conf.*, Nov. 2010, pp. 1193–1198.
[11] M. A. Davenport, P. T. Boufounos, M. B. Wakin, and R. G. Baraniuk, "Signal processing with compressive measurements," *IEEE J. Sel. Topics Signal Process.*, vol. 4, no. 2, pp. 445–460, Apr. 2010.
[12] J. Haupt and R. Nowak, "Compressive sampling for signal detection," in *Proc. Int. Conf. Acoust., Speech, Signal Process.*, 2007, vol. 3, pp. 1509–1512.
[13] J. Haupt and R. Nowak, A generalized restricted isometry property Univ. Wisconsin-Madison, Madison, USA, Dec. 2007, Tech. Rep. ECE-07-1.
[14] W. U. Bajwa, J. D. Haupt, A. M. Sayeed, and R. D. Nowak, "Joint source-channel communications for distributed estimation in sensor networks," *IEEE Trans. Inf. Theory*, vol. 53, no. 10, pp. 3629–3653, Oct. 2007.
[15] J. D. Haupt, W. U. Bajwa, M. Rabbat, and R. D. Nowak, "Compressed sensing for networked data," *IEEE Signal Process. Mag.*, vol. 25, no. 2, pp. 92–101, Mar. 2008.
[16] Y. Mostofi and P. Sen, "Compressive cooperative sensing and mapping in mobile networks," in *Proc. Amer. Control Conf.*, Jun. 2009, pp. 3387–3404.
[17] B. M. Sanandaji, T. L. Vincent, and M. B. Wakin, "Concentration of measure inequalities for compressive Toeplitz matrices with applications to detection and system identification," in *Proc. 49th IEEE Conf. Decis. Control*, Dec. 2010, pp. 2922–2929.
[18] M. B. Wakin, B. M. Sanandaji, and T. L. Vincent, "On the observability of linear systems from random, compressive measurements," in *Proc. 49th IEEE Conf. Decis. Control*, Dec. 2010, pp. 4447–4454.
[19] E. J. Candes, J. Romberg, and T. Tao, "Stable signal recovery from incomplete and inaccurate measurements," *Commun. Pure Appl. Math.*, vol. 59, no. 8, pp. 1207–1223, 2006.
[20] E. J. Candes, "The restricted isometry property and its implications in compressive sensing," *Comptes Rendus Mathematique*, vol. 346, no. 9–10, pp. 589–592, May 2008.
[21] M. A. Davenport and M. B. Wakin, "Analysis of orthogonal matching pursuit using the restricted isometry property," *IEEE Trans. Inf. Theory*, vol. 56, no. 9, pp. 4395–4401, Sep. 2010.
[22] S. Huang and J. Zhu, "Recovery of sparse signals using OMP and its variants: Convergence analysis based on RIP," *Inverse Probl.*, vol. 27, no. 3, Mar. 2011.
[23] R. Maleh, Improved RIP analysis of orthogonal matching pursuit [Online]. Available: http://arxiv.org/abs/1102.4311
[24] Q. Mo and Y. Shen, "A remark on the restricted isometry property in orthogonal matching pursuit," *IEEE Trans. Inf. Theory*, vol. 58, no. 6, pp. 3654–3656, Jun. 2012.
[25] M. A. Davenport, J. N. Laska, P. T. Boufounos, and R. G. Baraniuk, A simple proof that random matrix are democratic USA, Rice Univ.. Houston, TX, Nov. 2009, Tech. Rep..
[26] J. N. Laska, P. T. Boufounos, M. A. Davenport, and R. G. Baraniuk, "Democracy in action: Quantization, saturation, and compressive sensing," *Appl. Comput. Harmon. Anal.*, vol. 31, pp. 429–443, 2011.
[27] R. A. Horn and C. R. Johnson, *Matrix Analysis*. Cambridge, U.K.: Cambridge Univ. Press, 1985.
[28] M. E. Davies and R. Gribonval, "Restricted isometry constants where l^p sparse recovery can fail for $0 < p \leq 1$," *IEEE Trans. Inf. Theory*, vol. 55, no. 5, pp. 2203–2214, May 2009.
[29] S. Lang and G. Murraw, *Geometry*, 2nd ed. New York, USA: Springer-Verlag, 1988.
[30] F. E. Seymour and P. J. Smith, *Plane Geometry*. New York: Macmillan, 1949.
[31] C. Olsson, F. Kahl, and M. Oskarsson, "Branch-and-bound methods for Euclidean registration problems," *IEEE Trans. Pattern Anal. Mach. Intell.*, vol. 31, no. 5, pp. 783–794, May 2009.
[32] Y. Shen and H. Foroosh, "View-invariant action recognition using fundamental ratios," in *Proc. IEEE Conf. Comput. Vis. Pattern Recognit.*, 2008, pp. 1–8.
[33] L. H. Chang and J. Y. Wu, "Compressive-domain interference cancellation via orthogonal projection: How small the restricted isometry constant of the effective sensing matrix can be?," in *Proc. IEEE Wireless Commun. Network. Conf.*, Paris, France, 2012, pp. 256–261.
[34] A. Magen, "Dimensionality reductions that preserve volumes and distance to affine spaces, and their algorithmic applications," in *Randomization and Approximation Techniques in Computer Science*, ser. Lecture Notes in Computer Science. Berlin, Germany: Springer-Verlag, 2002, vol. 2483, pp. 239–253.
[35] A. Magen and A. Zouzias, "Near optimal dimensionality reduction that preserves volumes," in *Approximation, Randomization, and Combinatorial Optimization: Algorithms and Techniques*, ser. Lecture Notes in Computer Science. Berlin, Germany: Springer-Verlag, 2008, vol. 5171, pp. 523–534.
[36] L. H. Chang and J. Y. Wu, "Achievable angles between two compressed sparse vectors under RIP-induced norm/distance constraints," submitted to the *14th IEEE International Workshop on Signal Processing Advances in Wireless Communications*.

Ling-Hua Chang received the B. S. degree from the Department of Electrical and Computer Engineering, National Chiao Tung University, Taiwan, in 2010. She is currently a Ph. D. student in the Institute of Communications Engineering, National Chiao Tung University, Taiwan. Her research interests include signal processing and linear algebra.

Jwo-Yuh Wu received the B. S. degree in 1996, the M. S. degree in 1998, and the Ph. D. degree in 2002, all in Electrical and Control Engineering, National Chiao Tung University, Taiwan. During 2003 and 2007, he was a post doctor research fellow in the Department of Communications Engineering, National Chiao Tung University, Taiwan. Starting from 2008, he was an assistant professor in the Department of Electrical and Computer Engineering, and the Institute of Communications Engineering, National Chiao Tung University, Taiwan, where he has been an associate professor since 2011. His general research interests are in signal processing, wireless communications, control systems, linear algebra, and applied functional analysis.